Annals of Physics 324 (2009) 1105–1135

Contents lists available at ScienceDirect

Annals of Physics

journal homepage: www.elsevier.com/locate/aop

Non-equilibrium scaling analysis of the Kondo model with voltage bias

Peter Fritsch *, Stefan Kehrein

Physics Department, Arnold Sommerfeld Center for Theoretical Physics and Center for NanoScience, Ludwig-Maximilians-Universität München, Theresisenstr. 37, 80333 München, Germany

ARTICLE INFO

Article history:
Received 17 November 2008
Accepted 26 January 2009
Available online 5 February 2009

Keywords:
Kondo model
Non-equilibrium
Flow equations

ABSTRACT

The quintessential description of Kondo physics in equilibrium is obtained within a scaling picture that shows the buildup of Kondo screening at low temperature. For the non-equilibrium Kondo model with a voltage bias, the key new feature are decoherence effects due to the current across the impurity. In the present paper, we show how one can develop a consistent framework for studying the non-equilibrium Kondo model within a scaling picture of infinitesimal unitary transformations (flow equations). Decoherence effects appear naturally in third order of the β-function and dominate the Hamiltonian flow for sufficiently large voltage bias. We work out the spin dynamics in non-equilibrium and compare it with finite temperature equilibrium results. In particular, we report on the behavior of the static spin susceptibility including leading logarithmic corrections and compare it with the celebrated equilibrium result as a function of temperature.

© 2009 Elsevier Inc. All rights reserved.

1. Introduction

1.1. Motivation

Scaling concepts provide an invaluable tool in modern Theoretical Physics and are fundamentally important for understanding universal behavior and phase diagrams of quantum many-body systems. To date, most of these applications have been to equilibrium problems, where the basic idea of scaling to focus on the low-energy excitations of the system is most naturally applicable. Non-equilibrium problems, like systems prepared in an initial non-equilibrium state, or systems in a steady state far

* Corresponding author.
E-mail addresses: peter.fritsch@physik.lmu.de (P. Fritsch), stefan.kehrein@physik.lmu.de (S. Kehrein).

0003-4916/$ - see front matter © 2009 Elsevier Inc. All rights reserved.
doi:10.1016/j.aop.2009.01.004

from equilibrium (like transport processes between reservoirs), are already conceptually problematic for a scaling analysis since the focus cannot be on the low-energy excitations from the equilibrium ground state alone. A lot of theoretical work has recently been devoted to developing extension of scaling ideas to non-equilibrium problems, namely the frequency-dependent renormalization group [1,2], the real-time renormalization group [3,4], the Coulomb gas representation [5,6] and the flow equation approach [7,8].

This paper provides a detailed account of the flow equation approach applied to a non-equilibrium steady state of a quantum impurity model. Concretely, we study the Kondo model with a dc-voltage bias that produces a stationary current. This non-equilibrium Kondo model is a natural candidate for our analysis since it (i) can be realized experimentally in quantum dot experiments and (ii) its equilibrium version is the paradigm model for strong-coupling impurity physics in condensed matter theory. The current paper is a substantial extension of work previously presented in [7]. In particular, we study in detail the spin dynamics and the behavior of the static spin susceptibility χ_0 in non-equilibrium. We extend previous results in the literature, which, for example, allows us to compare the leading logarithmic corrections in non-equilibrium with the equilibrium result for $\chi_0(T)$.

The experimental motivation for our study is the observation of the Kondo effect in the Coulomb blockade regime of quantum dots, first realized in 1998 [9–11]. If a quantum dot that is weakly coupled to two leads is tuned into the Coulomb blockade regime such that it carries a net spin, resonant tunneling through the dot leads to a Kondoesque increase of the conductance up to the unitarity limit upon lowering temperature [12]. This was first predicted theoretically in [13,14]. The case of small voltage bias between the two leads, $V \ll T_K$, where T_K is the equilibrium Kondo temperature, can be analyzed using linear-response theory from the well-understood equilibrium ground state [13,14].

The case of intermediate voltage bias, $V \approx T_K$, that matches the linear-response to the large voltage bias regime, has until recently been out of reach for any controlled theoretical investigation. Very recently, new methods like the scattering state numerical renormalization group [15], the time-dependent density renormalization group [16], and the scattering state Bethe ansatz [17] have been developed that can access this crossover regime, though much more work needs to be done before a complete picture will emerge.

In this paper, we study the situation of large voltage bias, $V \gg T_K$, where one expects to find weak-coupling physics and therefore the possibility to do a controlled renormalized perturbation expansion. Kaminski et al. first developed a scaling picture of the large voltage bias Kondo model based on the invariance of the current under the RG-flow [18]. Subsequently, Rosch et al. developed a more sophisticated approach based on frequency-dependent vertices and Keldysh diagrammatics [1,2,19,20]. In both approaches, decoherence effects due to non-equilibrium spin relaxation processes generated by the stationary current play a key role: the resulting decoherence rate $\Gamma_{\mathrm{rel}} \propto V/\ln^2(V/T_K)$ [21] is essential for cutting off inter-lead scattering processes that are not immediately cut off by the voltage bias. The decoherence rate Γ_{rel} is therefore responsible for actually making the situation $V \gg T_K$ a weak-coupling problem. Such decoherence effects related to the noise produced in stationary non-equilibrium states are expected to be generically important in non-equilibrium problems.

The flow equation approach applied to the large voltage bias regime permits an analysis of this regime that is complimentary to the other approaches mentioned above: Here, the important decoherence effects emerge in a Hamiltonian scaling framework. We will improve the accuracy of some quantities using this approach, for example regarding the non-equilibrium dynamical spin susceptibility and the behavior of the static spin susceptibility as a function of the voltage bias. In addition, the Hamiltonian scaling picture developed here offers insights into non-equilibrium scaling in general.

The basic idea of the flow equation approach [22–24] is to make a Hamiltonian increasingly more band-diagonal by a suitable sequence of infinitesimal unitary transformations. Band-diagonality is here measured in terms of the energy transfer of scattering processes, therefore in the flow equation framework the flowing Hamiltonian $H(\Lambda_{\mathrm{feq}})$ at the "scale" Λ_{feq} only contains interaction matrix elements with energy transfer $|\Delta E| \lesssim \Lambda_{\mathrm{feq}}$. This should be compared with the conventional scaling approach where one integrates out Hilbert space states with an energy larger than some cutoff Λ_{RG}, and then successively lowers this cutoff. The essential idea behind both approaches is to organize a perturbative expansion in such a way as to first deal with large energy denominators and to avoid small

energy-denominators; this sequence allows for stable expansions even when dealing with non-perturbative energy scales like the Kondo temperature T_K.

However, one important conceptual difference between these two approaches is that the flow equation approach retains all states in the Hilbert space but decouples them, while the conventional scaling approach actually eliminates high-energy states. If one only focuses on the low-energy physics in an equilibrium problem, this difference is unimportant and the flow equation approach is consistent with the conventional RG-flow with the identification $\Lambda_{\rm feq} \propto \Lambda_{\rm RG}$ (explicit examples for this observation can be found in [25,26]). In a non-equilibrium situation like the Kondo model with voltage bias, the difference is, however, more fundamental. Fig. 1 schematically depicts the two schemes once the cutoff is reduced below the scale set by the voltage bias, $\Lambda < V$. In the flow equation framework, the Hamiltonian $H(\Lambda_{\rm feq})$ still describes the stationary current flowing across the dot, while scaling around the separate Fermi surfaces of the two leads does not allow for energy-diagonal transport processes across the dot anymore. Therefore, a naive application of the conventional scaling approach purports to eliminate scattering processes with small energy-denominators $|\Delta E| \ll \Lambda_{\rm RG}$ across the dot, which violates the spirit of renormalized perturbation theory. We will later see that it is precisely this point which allows us to understand qualitatively and quantitatively non-equilibrium decoherence in a Hamiltonian framework.

1.2. Outline

This paper is organized as follows. In Section 2, we define the model and briefly review its conventional scaling analysis. In Section 3.1, we first introduce the flow equation method, and then in part 3.2 apply it to a general Kondo model Hamiltonian with an arbitrary number of leads with or without voltage bias. This is the core part of our calculation. The resulting equations are then analyzed in equilibrium in part 3.3, where we reproduce the conventional two-loop β-function. In parts 3.4 and 3.5, we then specialize to the case of interest in this paper; the Kondo model with two leads and voltage bias V. Using these flow equations, we work out and analyze the scaling picture of the Kondo model with voltage bias in Section 4. Section 5 discusses our results for the spin dynamics in non-equilibrium, which are compared with the well-known equilibrium behavior at non-zero temperature. In particular, Sections 5.3 and 5.4 contain the key new results of this work regarding the spin dynamics and the static spin susceptibility in non-equilibrium. A summary of results and conclusions is presented in Section 6. Appendix A contains important commutators and normal-ordering results that are frequently needed, and Appendix A.3 contains details of the numerical solution of the flow equations.

2. The Kondo model with voltage bias

2.1. Model

We are investigating a quantum dot that can be modelled by a spin-1/2 degree of freedom $\vec{S}$ coupled to conduction electrons in a left (l) and a right (r) lead with no external magnetic field

$$H = \sum_{a,p,\alpha} (\epsilon_p - \mu_a) c^\dagger_{ap\alpha} c_{ap\alpha} + \sum_{a',a} J_{a'a} \sum_{p',p} \vec{S} \cdot \vec{s}_{(a'p')(ap)} . \tag{1}$$

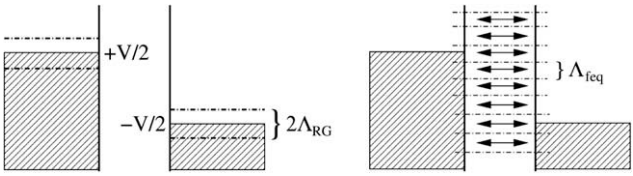

Fig. 1. Left: Conventional scaling picture where states are integrated out around the two Fermi surfaces with voltage bias V (here depicted for cutoff $\Lambda_{\rm RG} < V$). Right: Flow equation approach. Here, all scattering processes with energy transfer $|\Delta E| \lesssim \Lambda_{\rm feq}$ are retained in $H(\Lambda_{\rm feq})$.

Here, $a\prime, a = l, r$ label the two leads, $p\prime, p$ are momentum labels, and the chemical potentials are given by $\mu_{l,r} = \pm V/2$. The conduction band electron spin operators are defined by $\vec{s}_{(a'p')(ap)} = \frac{1}{2}\sum_{\alpha,\beta} c^\dagger_{a'p'\alpha}\vec{\sigma}_{\alpha\beta}c_{ap\beta}$, where $\vec{\sigma}$ are the Pauli matrices. The couplings $J_{a'a}$ describe the exchange interaction with the localized spin degree of freedom, with $J_{lr} = J_{rl}$ for hermiticity. If the quantum dot can be described by an Anderson impurity model with tunneling rates $\Gamma_{l,r}$ from the left/right lead, the coupling constants of our effective Kondo model are related by $J^2_{lr} = J_{ll}J_{rr}$ and $J_{ll}/J_{rr} = \Gamma_l/\Gamma_r$ [18]. We define $r \stackrel{\text{def}}{=} \Gamma_l/\Gamma_r$ as the *asymmetry parameter* of our model. We will derive the scaling equations without making any of the above assumptions so that also more general complex quantum dot structures can be investigated (e.g., in double dot systems the relation $J^2_{lr} = J_{ll}J_{rr}$ is not necessarily fulfilled). We assume a linear dispersion relation leading to a constant conduction band density of states ρ and introduce the dimensionless coupling constants $g_l = \rho J_{ll}$, $g_r = \rho J_{rr}$ and $g_t = \rho J_{lr}$ (t for transport). The band cutoff is denoted by D and we are only interested in the universal behavior on energy scales much smaller than D.

2.2. Conventional scaling analysis

Below, we will sum up the results of the conventional scaling analysis for the non-equilibrium Kondo model in the spirit of Fig. 1, that is reminiscent of Anderson's "poor man's scaling" in equilibrium [27]. The derivation of the one-loop results is straightforward, see [18,28]. Upon lowering the cutoff Λ_{RG} around the two Fermi surfaces, but while $\Lambda_{\text{RG}} \gtrsim V$ still holds, one finds the equilibrium scaling equations

$$\frac{dg_l}{d\ln\Lambda_{\text{RG}}} = -g_l^2 - g_t^2, \tag{2}$$

$$\frac{dg_r}{d\ln\Lambda_{\text{RG}}} = -g_r^2 - g_t^2, \tag{3}$$

$$\frac{dg_t}{d\ln\Lambda_{\text{RG}}} = -g_t(g_l + g_r), \tag{4}$$

plus third-order terms in the coupling constants. Once the cutoff is reduced below the voltage bias, $\Lambda_{\text{RG}} \lesssim V$, the strong-coupling scaling of the coupling g_t stops since there is no sharp Fermi surface for transport processes on this scale. Similarly, only the inter-lead scattering processes still contribute to the scaling equations of g_l and g_r:

$$\frac{dg_l}{d\ln\Lambda_{\text{RG}}} = -g_l^2, \tag{5}$$

$$\frac{dg_r}{d\ln\Lambda_{\text{RG}}} = -g_r^2, \tag{6}$$

$$\frac{dg_t}{d\ln\Lambda_{\text{RG}}} = 0. \tag{7}$$

We now assume that the Kondo model can be derived from an underlying Anderson impurity model, and one easily solves the equation for g_t down to the infrared limit [18]

$$g_t(\Lambda_{\text{RG}} = 0) = \frac{\sqrt{\Gamma_l\Gamma_r}}{\Gamma_l + \Gamma_r}\frac{1}{\ln(V/T_{\text{K}})}, \tag{8}$$

where $T_{\text{K}} = D\exp(-1/g_l + g_r)$ is the Kondo temperature of the equilibrium model (i.e., for $V = 0$). The IR-coupling (8) determines the current I across the dot and a conventional second-order Keldysh calculation in the renormalized quantities yields [18] $I = (3\pi/4)Vg_t^2(\Lambda_{\text{RG}} = 0)$. This leads to perturbative result for the differential conductance $G(V)$ valid in the limit $V \gg T_{\text{K}}$:

$$G(V) = G_u\frac{3\pi^2}{16\ln^2(V/T_{\text{K}})}, \tag{9}$$

where

$$G_u = \frac{2e^2}{h}\frac{4\Gamma_l\Gamma_r}{(\Gamma_l + \Gamma_r)^2} = \frac{2e^2}{h}\frac{4}{(1+r)(1+r^{-1})} \tag{10}$$

is the conductance in the unitarity limit.

Notice that there is no IR-cutoff mechanism for the inter-lead scattering processes in the scaling equations (5) and (6) for g_l, g_r, which therefore yield strong-coupling divergences even for large voltage bias [28]. However, Rosch et al. have pointed out the importance of spin relaxation processes due to the stationary current [21]. Second-order perturbation theory in the renormalized quantities yields the decoherence rate

$$\Gamma_{\rm rel} \propto \frac{V}{\ln^2(V/T_{\rm K})}, \tag{11}$$

which cuts off the inter-lead strong-coupling flow and eliminates the possibility of two-channel Kondo physics in Kondo dots that can be derived from an underlying Anderson impurity model. The observation that the non-equilibrium Kondo model becomes a weak-coupling problem for $\Gamma_{\rm rel} \gg T_{\rm K}$ has then been exploited to derive a number of physically relevant quantities like the conduction electron T-matrix, the non-equilibrium magnetization and the conductance both with and without an external magnetic field [1,2,19,20].

3. Flow equation analysis

3.1. Flow equation method

The basic idea of the flow equation approach [22–24] is to make a many-particle Hamiltonian increasingly more diagonal through a sequence of infinitesimal unitary transformations. Such a flow can be generated by the differential equation

$$\frac{dH(B)}{dB} = [\eta(B), H(B)] \tag{12}$$

with some suitable antihermitean generator $\eta(B)$; Eq. (12) then generates a one-parameter family of unitarily equivalent Hamiltonians $H(B)$. We set $H(B=0)$ as the initial Hamiltonian and want $H(B=\infty)$ to be the final diagonal Hamiltonian. In order to generate a stable expansion, it is of fundamental importance to properly deal with energy-scale separation during the flow, similar to conventional scaling approaches. For small B (initial phase of the flow), we will decouple modes with large energy differences, while later for large flow parameter B we will deal with increasingly more energy-diagonal processes. This sequence of transformations is generically generated by the "canonical" generator suggested by Wegner [22]

$$\eta(B) \stackrel{\rm def}{=} [H_0(B), H_{\rm int}(B)], \tag{13}$$

where $H_0(B)$ is the diagonal part of the Hamiltonian $H(B)$ and $H_{\rm int}(B)$ its interaction part. The flow parameter B then has the dimension $(\text{Energy})^{-2}$, and $\Lambda_{\rm feq} \stackrel{\rm def}{=} B^{-1/2}$ is the flow equation energy scale that expresses how energy-diagonal the Hamiltonian $H(B)$ has become. Interaction matrix elements with energy transfer $|\Delta E| \gtrsim \Lambda_{\rm feq}$ are eliminated in $H(\Lambda_{\rm feq})$, while processes with $|\Delta E| \lesssim \Lambda_{\rm feq}$ are still retained. We will use the notation with B or $\Lambda_{\rm feq}$ interchangeably.

The flow equation approach has been successfully applied to numerous equilibrium many-body problems, like dissipative quantum systems [29,30], the two-dimensional Hubbard model [31], low-dimensional spin systems [32], and strong-coupling models like the Sine–Gordon model [25] or the Kondo model [26,33]. Due to its intrinsic energy scale separation, the flow equation method generates the same IR-scaling flow as conventional renormalization group methods, with the identification $\Lambda_{\rm feq} \propto \Lambda_{\rm RG}$. Notice that in certain strong-coupling problems [25,26] the flow equation approach even allows a controlled systematic expansion in the strong-coupling phase where conventional scaling leads to a strong-coupling divergence.

The main conceptual difference between flow equations and the conventional scaling approach is that in the flow equation approach the Hilbert space remains unchanged while modes become *decoupled*, whereas in the scaling approach high-energy modes are successively integrated out, compare Fig. 2. This allows one to evaluate correlation functions on all energy scales within the flow equation

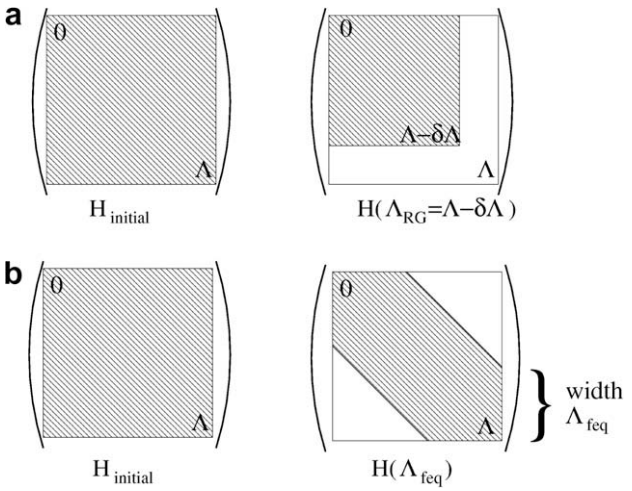

Fig. 2. (a) Schematic picture of the conventional scaling approach where states with energies $[\Lambda_{\mathrm{RG}} - \delta\Lambda_{\mathrm{RG}}, \Lambda_{\mathrm{RG}}]$ are integrated out. (b) Flow equation approach. Here, all scattering processes with energy transfer $|\Delta E| \gtrsim \Lambda_{\mathrm{feq}}$ are eliminated in $H(\Lambda_{\mathrm{feq}})$. The shaded areas in (a) and (b) schematically indicate non-vanishing interaction matrix elements.

framework [26,29], however, for non-equilibrium problems this conceptual difference will turn out to be even more fundamental as we will see later (compare also Fig. 1). Applications of the flow equation approach to non-equilibrium initial state problems have been discussed in [8,34,35]. In the sequel, we will explain in detail the flow equation analysis of the stationary non-equilibrium problem provided by the Kondo model with voltage bias.

3.2. Kondo model

For an interacting many-body problem like the Kondo Hamiltonian (1) the flow equation approach generates higher and higher-order interaction terms in the commutators (12) and (13). Similar to a conventional scaling analysis, the flow therefore needs to be approximated by an expansion in a suitable expansion parameter that remains sufficiently small during the entire flow. In our problem, we will use the running coupling constants $J(B)$ as our expansion parameters [36] and perform a consistent systematic expansion in orders of $J(B)$. No further input except this systematic expansion is required to find both coherent *and* decoherence effects in our non-equilibrium problem in a systematic controlled expansion. Since we are performing unitary transformations (12) which do not explicitly depend on the ground state of the system (though implicitly as we will see below), it is actually advantageous to first derive the differential flow equations for a general Kondo Hamiltonian with couplings to some arbitrary number of leads (with arbitrary chemical potentials). We introduce a general index t labelling the conduction band electrons and write

$$H = \sum_{t,\alpha} \epsilon_t c^\dagger_{t\alpha} c_{t\alpha} + \sum_{t',t} J_{t't} \vec{S} \cdot \vec{s}_{t't} \tag{14}$$

with $J_{t't} = J_{tt'}$ for hermiticity. This will allow us to study both the equilibrium model without voltage bias and the non-equilibrium model on the same footing. In the equilibrium model, there is only one lead, therefore $t = p$ with electron momentum p, whereas in the Kondo model with voltage bias the label t is a multi-index labelling both lead left/right and electron momentum, $t = (a, p)$ with $a = l, r$.

3.2.1. $H(B)$ and generator $\eta(B)$

During the flow equation procedure new interaction terms are generated that are not present in the initial Hamiltonian (14). We will neglect the newly generated normal-ordered terms in $O(J^3)$ and high-

er in $H(B)$, which can only affect our scaling equations for the couplings $J(B)$ in order J^4 and higher (since the commutator (12) always increases the order by at least one). We will later see that this order of the flow equation calculation is the minimum order necessary to obtain a controlled expansion in the sense that the flowing coupling constants remain finite for $V \gg T_K$. Higher order calculations beyond our present work can be understood as corrections to the results presented here.

Within our order of the calculation, the flowing Hamiltonian can be parametrized as

$$H(B) = \sum_{t,\alpha} \epsilon_t c^\dagger_{t\alpha} c_{t\alpha} + \sum_{t',t} J_{t't}(B) \vec{S} \cdot \vec{s}_{t't} + i \sum_{t',t,u',u} K_{t't,u'u}(B) : \vec{S} \cdot (\vec{s}_{t't} \times \vec{s}_{u'u}) :, \tag{15}$$

where $K_{t't,u'u}(B)$ will turn out to be the only newly generated term in $O(J^2)$. It obeys $K_{t't,u'u}(B) = -K_{tt',uu'}(B)$ for hermiticity and initially $K_{t't,u'u}(B=0) = 0$. In (15), $: \ldots :$ denotes normal-ordering with respect to the ground state of the system without Kondo impurity. We use the normal-ordering procedure as introduced in [22] (for more details see the appendix). Notice that we do not need to explicitly normal-order the term proportional to $J_{t't}$ in (15) since it automatically appears in its normal-ordered form.

The generator of the infinitesimal unitary transformations is given by (13), where the diagonal part of $H(B) = H_0 + H_{\text{int}}(B)$ is the conduction band kinetic energy $H_0 = \sum_{t,\alpha} \epsilon_t c^\dagger_{t\alpha} c_{t\alpha}$. This leads to

$$\eta = \sum_{t',t} \eta^{(1)}_{t't} \vec{S} \cdot \vec{s}_{t't} + i \sum_{t',t,u',u} \eta^{(2)}_{t't,u'u} : \vec{S} \cdot (\vec{s}_{t't} \times \vec{s}_{u'u}) : \tag{16}$$

where

$$\eta^{(1)}_{t't} = (\epsilon_{t'} - \epsilon_t) J_{t't}, \tag{17}$$

$$\eta^{(2)}_{t't,u'u} = (\epsilon_{t'} + \epsilon_{u'} - \epsilon_t - \epsilon_u) K_{t't,u'u}. \tag{18}$$

Here and in the sequel, we will usually suppress the explicit B-dependence of all parameters and coupling constants in our notation.

3.2.2. Terms in $O(J)$ and $O(J^2)$

In order to work out the unitary flow of the Hamiltonian (12) we now need to calculate the commutator $[\eta(B), H(B)]$. This is the main calculational problem of the flow equation approach. For the current problem we will now proceed order by order in the coupling constant J with this calculation.

Let us first evaluate $[\eta(B), H_0]$. This is straightforward and leads to

$$[\eta, H_0] = \sum_{t',t} (\epsilon_t - \epsilon_{t'}) \eta^{(1)}_{t't} \vec{S} \cdot \vec{s}_{t't} + i \sum_{t',t,u',u} (\epsilon_t + \epsilon_u - \epsilon_{t'} - \epsilon_{u'}) \eta^{(2)}_{t't,u'u} : \vec{S} \cdot (\vec{s}_{t't} \times \vec{s}_{u'u}) : . \tag{19}$$

Next, we need to find $[\eta(B), H_{\text{int}}(B)]$. We first identify its contributions in order J^2, which can only come from

$$C_2 = \left[\sum_{t',t} \eta^{(1)}_{t't} \vec{S} \cdot \vec{s}_{t't}, \sum_{u',u} J_{u'u} \vec{S} \cdot \vec{s}_{u'u} \right]. \tag{20}$$

The basic commutator $[\vec{S} \cdot \vec{s}_{t't}, \vec{S} \cdot \vec{s}_{u'u}]$ is worked out in the appendix and given in (116). Inserting it in (20) yields

$$\begin{aligned} C_2 = {} & i \sum_{t',t,u,u'} (\epsilon_{t'} - \epsilon_t) J_{t't} J_{u'u} : \vec{S} \cdot (\vec{s}_{t't} \times \vec{s}_{u'u}) : + \sum_{t',t,v} (\epsilon_{t'} + \epsilon_t - 2\epsilon_v) J_{t'v} J_{vt} (n(v) - 1/2) \vec{S} \cdot \vec{s}_{t't} \\ & + \frac{3}{16} \sum_{t',t,v,\alpha} (\epsilon_{t'} + \epsilon_t - 2\epsilon_v) J_{t'v} J_{vt} : c^\dagger_{t'\alpha} c_{t\alpha} : \end{aligned} \tag{21}$$

plus an uninteresting constant that does not contribute to the further flow. Here we have defined the expectation value with respect to the non-interacting ground state

$$n(v) \stackrel{\text{def}}{=} \langle c^\dagger_{v\alpha} c_{v\alpha} \rangle, \tag{22}$$

which is just the occupation number. No summation over α is implied in this definition.

Comparing coefficients in (15), (19) and (21), we find the following differential flow equations:

$$\frac{dJ_{t't}}{dB} = -(\epsilon_{t'} - \epsilon_t)^2 J_{t't} + \sum_v (\epsilon_{t'} + \epsilon_t - 2\epsilon_v) J_{t'v} J_{vt} (n(v) - 1/2) + O(J^3), \tag{23}$$

$$\frac{dK_{t't,u'u}}{dB} = -(\epsilon_{t'} + \epsilon_{u'} - \epsilon_t - \epsilon_u)^2 K_{t't,u'u} - (\epsilon_{u'} - \epsilon_u) J_{t't} J_{u'u} + O(J^3). \tag{24}$$

From (21), one would conclude that a new term

$$\sum_{t',t} \sum_{\alpha} V_{t't}(B) : c^\dagger_{t'\alpha} c_{t\alpha} : \tag{25}$$

is generated in the Hamiltonian $H(B)$ that has not been included so far

$$\frac{dV_{t't}}{dB} = \frac{3}{16} \sum_v (\epsilon_{t'} + \epsilon_t - 2\epsilon_v) J_{t'v} J_{vt} + O(J^3). \tag{26}$$

However, we will see below that this contribution vanishes identically due to symmetry reasons (in fact, it only appears in $O(J^4)$).

3.2.3. Terms in $O(J^3)$

Our goal is to derive the β-function of the Kondo model up to two-loop order within the flow equation framework. This implies that we need to calculate the terms in order J^3 that contribute to the differential equation (23) for $J_{t't}(B)$. Notice that our differential equation for $K_{t't,u'u}(B)$ generates this term (which is not present for $B = 0$) in order J^2. Also notice that we do not need to calculate its $O(J^3)$-contribution because this can only feed back into the differential equation for $J_{t't}(B)$ in $O(J^4)$. We are therefore left with identifying the terms with structure $\vec{S} \cdot \vec{s}_{t't}$ in the normal-ordered commutators

$$C_{3'} = \left[\sum_{u',u} \eta^{(1)}_{u'u} \vec{S} \cdot \vec{s}_{u'u}, i \sum_{v',v,w',w} K_{v'v,w'w} : \vec{S} \cdot (\vec{s}_{v'v} \times \vec{s}_{w'w}) : \right] \tag{27}$$

and

$$C_{3''} = \left[i \sum_{v',v,w',w} \eta^{(2)}_{v'v,w'w} : \vec{S} \cdot (\vec{s}_{v'v} \times \vec{s}_{w'w}) :, \sum_{u',u} J_{u'u} \vec{S} \cdot \vec{s}_{u'u} \right]. \tag{28}$$

We can combine these two contributions into

$$C_3 = \sum (\epsilon_{u'} - \epsilon_u - \epsilon_{v'} + \epsilon_v - \epsilon_{w'} + \epsilon_w) J_{u'u} K_{v'v,w'w} i [\vec{S} \cdot \vec{s}_{u'u}, : \vec{S} \cdot (\vec{s}_{v'v} \times \vec{s}_{w'w}) :]. \tag{29}$$

The commutator $[\vec{S} \cdot \vec{s}_{u'u}, : \vec{S} \cdot (\vec{s}_{v'v} \times \vec{s}_{w'w}) :]$ is worked out in the appendix and given in (122). We only need the contribution with structure $\vec{S} \cdot \vec{s}_{t't}$ and inserting yields

$$C_3 = \frac{1}{2} \sum (2\epsilon_u - 2\epsilon_{u'} + \epsilon_t - \epsilon_{t'}) \vec{S} \cdot \vec{s}_{t't} J_{u'u} (K_{u'u,t't} - K_{t't,u'u}) (n(u')(1 - n(u)) + n(u)(1 - n(u'))). \tag{30}$$

We have now derived all the necessary terms to write down the flow equations to the desired order.

3.2.4. Flow equations

We include the term (30) in the differential equation (23) and find the following set of flow equations that completely determine the flow of the Hamiltonian $H(B)$ up to the resp. order in J:

$$\begin{aligned} \frac{dJ_{t't}}{dB} = & -(\epsilon_{t'} - \epsilon_t)^2 J_{t't} + \sum_v (\epsilon_{t'} + \epsilon_t - 2\epsilon_v) J_{t'v} J_{vt} (n(v) - 1/2) \\ & + \frac{1}{2} \sum_{u',u} (2\epsilon_u - 2\epsilon_{u'} + \epsilon_t - \epsilon_{t'}) J_{u'u} (K_{u'u,t't} - K_{t't,u'u}) (n(u')(1 - n(u)) + n(u)(1 - n(u'))) + O(J^4), \end{aligned} \tag{31}$$

$$\frac{dK_{t't,u'u}}{dB} = -(\epsilon_{t'} + \epsilon_{u'} - \epsilon_t - \epsilon_u)^2 K_{t't,u'u} - (\epsilon_{u'} - \epsilon_u) J_{t't} J_{u'u} + O(J^3). \tag{32}$$

In order to complete our analysis, we finally need to show that the terms $V_{t't}(B)$ from (25) indeed vanish to the required order. This is straightforward by solving (31) in linear order

$$J_{t't}(B) = (J_{t't}(B=0) + O(J^2))e^{-B(\epsilon_{t'}-\epsilon_t)^2} \tag{33}$$

and inserting in (26)

$$\frac{dV_{t't}}{dB} = \frac{3}{16}\sum_v J_{t'v}(B=0)J_{vt}(B=0)(\epsilon_{t'}+\epsilon_t-2\epsilon_v)e^{-B((\epsilon_{t'}-\epsilon_v)^2+(\epsilon_v-\epsilon_t)^2)} + O(J^3). \tag{34}$$

Since we assume a linear dispersion relation and initial coupling constants $J_{t't}(B=0)$ that are constant (at least in the low-energy limit), we only need to know

$$\sum_v (\epsilon_{t'}+\epsilon_t-2\epsilon_v)e^{-B((\epsilon_{t'}-\epsilon_v)^2+(\epsilon_v-\epsilon_t)^2)} = 0, \tag{35}$$

which holds up to possible band edge effects that do not influence the universal low-energy physics for $T_K \ll D$. Therefore

$$\frac{dV_{t't}}{dB} = O(J^3) \tag{36}$$

and the $V_{t't}$-terms do not influence the flow equations (31) and (32) in the orders that we are interested in. In fact, a more detailed analysis shows that even the $O(J^3)$-terms on the rhs of (36) vanish; the first non-vanishing contributions arise in order J^4.

Eqs. (31) and (32) constitute the main computational results of this paper and will now be analyzed in various settings. Notice that they apply for a general spin-1/2 multi-lead Kondo model, where we did not yet have to specify whether the system is equilibrium or not. The derivation of these equations followed from a straightforward application of the canonical flow equation framework as an expansion in powers of the flowing coupling constants. Also notice that the linear terms in (31) and (32) generate the canonical exponential decay of the coupling constants (33) that make the Hamiltonian $H(B)$ increasingly diagonal in energy space (see Fig. 2) with the identification $\Lambda_{\text{feq}} = B^{-1/2}$.

3.3. Equilibrium model

As a consistency check and in order to gain some insight into the system of flow equations, we now first analyze the equilibrium Kondo model at zero temperature $T = 0$. Here, the index t labelling the conduction band electrons in (14) only consists of the electron momentum and we have one exchange coupling J. We use the following approximate parametrization of the running couplings as a function of B:

$$\rho J_{p'p}(B) = g(B)e^{-B(\epsilon_{p'}-\epsilon_p)^2}, \tag{37}$$

where $g(B)$ is determined from the flow in the IR-limit $\epsilon_{p'} = \epsilon_p = 0$ (we choose $\epsilon_F = 0$). This parametrization is asymptotically correct in the IR-limit and we can identify $g(B)$ with the dimensionless running coupling constant of the conventional scaling approach.

Inserting the parametrization (37) into the flow equation (31) for $\epsilon_{p'} = \epsilon_p = 0$,

$$\frac{dg}{dB} = g^2\int_{-\infty}^{\infty} d\epsilon\, e^{-2B\epsilon^2}(-2\epsilon)(n(\epsilon)-1/2) + \int_{-\infty}^{0} d\epsilon' \int_0^{\infty} d\epsilon\, 2(\epsilon-\epsilon')ge^{-B(\epsilon'-\epsilon)^2}(K_{\epsilon'\epsilon,00} - K_{00,\epsilon'\epsilon}), \tag{38}$$

where we have inserted the zero temperature occupation numbers

$$n(\epsilon) = \Theta(-\epsilon). \tag{39}$$

Eq. (38) is integrated starting from $B = D^{-2}$, where D is the conduction band width (UV-cutoff). We also need to the flow of the K-terms that are initially not present in the Hamiltonian but generated during the flow: from (32) we deduce

$$\frac{dK_{\epsilon'\epsilon,00}}{dB} = 0, \tag{40}$$

$$\frac{dK_{00,\epsilon'\epsilon}}{dB} = -(\epsilon' - \epsilon)^2 K_{00,\epsilon'\epsilon} - g^2 e^{-B(\epsilon'-\epsilon)^2}(\epsilon' - \epsilon) \tag{41}$$

Eq. (41) can be solved easily

$$K_{00,\epsilon'\epsilon}(B) = -(\epsilon' - \epsilon)e^{-B(\epsilon'-\epsilon)^2}\int_0^B dB'\, g^2(B'). \tag{42}$$

From the scaling equation in second order for $g(B)$, one obtains the well-known slow logarithmic increase during the flow, therefore the integral in (42) is dominated by large values of B' and one can write

$$K_{00,\epsilon'\epsilon}(B) = -(\epsilon' - \epsilon)e^{-B(\epsilon'-\epsilon)^2}B(g^2(B) + O(g^3)). \tag{43}$$

Putting everything together in (38) and performing the remaining integrations, we obtain

$$\frac{dg}{dB} = \frac{g^2}{2B} - \frac{g^3}{4B} + \frac{O(g^4)}{B}. \tag{44}$$

In terms of the scaling parameter $\Lambda_{\mathrm{feq}} = B^{-1/2}$ with dimension energy, one can alternatively write

$$\frac{dg}{d\ln\Lambda_{\mathrm{feq}}} = -\beta^{(\mathrm{eq})}(g) \tag{45}$$

with the correct equilibrium β-function to two-loop order [37]

$$\beta^{(\mathrm{eq})}(g) = g^2 - \frac{1}{2}g^3 + O(g^4). \tag{46}$$

As expected for the equilibrium model, it therefore makes no difference whether one derives the IR-behavior with respect to the conventional scaling parameter Λ_{RG} or the flow equation scaling parameter Λ_{feq} (see Fig. 2). In the next section, we will explore how these results change in the non-equilibrium situation.

3.4. Non-equilibrium model (general parameters)

For the non-equilibrium setting with voltage bias V between the left and right lead the label t in (14) is a multi-index $t = (a, p)$ labelling both left/right lead ($a = l, r$) and electron momentum p. We choose the Fermi energy of the left lead to be $+V/2$ and of the right lead to be $-V/2$, therefore we have a current flowing from left to right. For now we will only look at zero temperature $T = 0$.

In our flow equations (31) and (32), we have to differentiate between the various scattering processes between the leads:

$$\begin{aligned}\frac{dJ_{(a'p')(ap)}}{dB} = &-(\epsilon_{p'} - \epsilon_p)^2 J_{(a'p')(ap)} + \sum_{b=l,r}\sum_q (\epsilon_{p'} + \epsilon_p - 2\epsilon_q) J_{(a'p')(bq)} J_{(bq)(ap)}(n_b(q) - 1/2) \\ &+ \frac{1}{2}\sum_{b',b=l,r}\sum_{q',q}(2\epsilon_q - 2\epsilon_{q'} + \epsilon_p - \epsilon_{p'}) J_{(b'q')(bq)}(K_{(b'q')(bq),(a'p')(ap)} - K_{(a'p')(ap),(b'q')(bq)})(n_{b'}(q')(1 - n_b(q)) \\ &+ n_b(q)(1 - n_{b'}(q'))) + O(J^4)\end{aligned} \tag{47}$$

for $a', a = l, r$ and

$$\frac{dK_{(a'p')(ap),(b'q')(bq)}}{dB} = -(\epsilon_{p'} + \epsilon_{q'} - \epsilon_p - \epsilon_q)^2 K_{(a'p')(ap),(b'q')(bq)} - (\epsilon_{q'} - \epsilon_q) J_{(a'p')(ap)} J_{(b'q')(bq)} + O(J^3) \tag{48}$$

for $b', b, a', a = l, r$. The effect of the voltage bias enters here only through the different ground state expectation values in the left and right lead

$$n_l(\epsilon) = \Theta(-\epsilon + V/2), \quad n_r(\epsilon) = \Theta(-\epsilon - V/2). \tag{49}$$

3.5. Non-equilibrium model ($J_{lr}^2 = J_{ll}J_{rr}$)

Eqs. (47) and (48) can be simplified considerably if the Kondo model can be derived from an underlying Anderson single impurity model. As explained in Section 2.1, the coupling constants then fulfill the relations $J_{lr}^2 = J_{ll}J_{rr}$ and $J_{ll}/J_{rr} = \Gamma_l/\Gamma_r = r$. Notice that the impurity physics is invariant under the exchange $r \leftrightarrow 1/r$ since this just amounts to an exchange of the two leads. One can verify easily that the impurity spin only couples to the following linear combination of left and right lead fermion operators

$$f_{p\alpha} \stackrel{\text{def}}{=} \frac{1}{\sqrt{1+r}} c_{rp\alpha} + \frac{1}{\sqrt{1+r^{-1}}} c_{lp\alpha}, \tag{50}$$

which obey the usual anticommuation relations $\{f_{p\alpha}, f_{p'\beta}^\dagger\} = \delta_{pp'}\delta_{\alpha\beta}$. The flowing Hamiltonian then takes the form

$$H(B) = \sum_{p,\alpha} \epsilon_p f_{p\alpha}^\dagger f_{p\alpha} + \sum_{p',p} J_{p'p}(B)\vec{S}\cdot\vec{s}_{p'p} + i\sum_{p',p,q',q} K_{p'p,q'q}(B) : \vec{S}\cdot(\vec{s}_{p'p}\times\vec{s}_{q'q}) :, \tag{51}$$

with the conduction band spin operators $\vec{s}_{p'p} = \frac{1}{2}\sum_{\alpha,\beta} f_{p'\alpha}^\dagger \vec{\sigma}_{\alpha\beta} f_{p\beta}$ defined for the f-operators. Eqs. (47) and (48) simplify to the following form where the external leads do not appear explicitly:

$$\begin{aligned}\frac{dJ_{p'p}}{dB} = & -(\epsilon_{p'}-\epsilon_p)^2 J_{p'p} + \sum_q (\epsilon_{p'}+\epsilon_p-2\epsilon_q) J_{p'q}J_{qp}(n_f(q)-1/2) + \frac{1}{2}\sum_{q',q}(2\epsilon_q - 2\epsilon_{q'}+\epsilon_p-\epsilon_{p'}) \\ & \times J_{q'q}(K_{q'q,p'p}-K_{p'p,q'q})(n_f(q')(1-n_f(q)) + n_f(q)(1-n_f(q'))) + O(J^4),\end{aligned} \tag{52}$$

$$\frac{dK_{p'p,q'q}}{dB} = -(\epsilon_{p'}+\epsilon_{q'}-\epsilon_p-\epsilon_q)^2 K_{p'p,q'q} - (\epsilon_{q'}-\epsilon_q)J_{p'p}J_{q'q} + O(J^3). \tag{53}$$

Here we have the initial condition $J_{p'p}(B=0) = J_{ll} + J_{rr}$ and the zero temperature Fermi distribution function for the f-operators

$$\begin{aligned} n_f(p) &= \langle f_{p\alpha}^\dagger f_{p\alpha}\rangle \\ &= \frac{1}{1+r} n_r(p) + \frac{1}{1+r^{-1}} n_l(p) \qquad (54) \\ &= \begin{cases} 0 & \epsilon_p > \frac{V}{2}, \\ \frac{1}{1+r^{-1}} & |\epsilon_p| \leqslant \frac{V}{2}, \\ 1 & \epsilon_p < -\frac{V}{2}. \end{cases} \qquad (55)\end{aligned}$$

In the sequel, we will restrict ourselves to the analysis of (52) and (53), that is we only investigate a Kondo model that can be realized from an underlying single Anderson impurity model.

4. Scaling picture of the Kondo model with voltage bias

4.1. IR-parametrization

Eqs. (52) and (53) contain the full information about the Hamiltonian flow to the resp. order in the coupling constant. We will analyze these equations both numerically and analytically to understand the scaling behavior of the non-equilibrium Kondo model. In order to get some first insights, we first perform an analytical analysis that is based on some additional approximations. However, we will later see that these approximations are justified with very good accuracy by comparison with the exact numerical solution.

The flow equation differential equations are connected with conventional scaling equations by using an approximation of the following form:

$$\rho J_{p'p}(B) = u_{\overline{p'p}}(B) e^{-B(\epsilon_{p'}-\epsilon_p)^2}, \tag{56}$$

which parametrizes the couplings in terms of the dimensionless running coupling constants $u_{\overline{p'p}}(B)$ on an averaged energy scale $\epsilon_{\overline{p'p}} \stackrel{\text{def}}{=} (\epsilon_{p'} + \epsilon_p)/2$. (In fact one can choose any energy in $[\min(\epsilon_p, \epsilon_{p'}), \max(\epsilon_p, \epsilon_{p'})]$ with excellent accuracy.) This ansatz solves the linear part of the flow equation (52) and allows us to perform the summations over q in closed form. One finds

$$\frac{du_p}{dB} = \frac{u_p^2}{2B}\left(\frac{1}{1+r}e^{-2B(-\epsilon_p - V/2)^2} + \frac{1}{1+r^{-1}}e^{-2B(-\epsilon_p + V/2)^2}\right) - 2\int d\epsilon_{q'}\, d\epsilon_q (\epsilon_{q'} - \epsilon_q)^2 u_q e^{-2B(\epsilon_{q'} - \epsilon_q)^2} \times \int_0^B dB'\, u_p(B') u_q(B') n_f(q')(1 - n_f(q)). \tag{57}$$

In the cubic term, a whole range of values $q\prime, q$ contributes to the integral where the product of the Fermi functions is non-zero. Again with very good accuracy, we can replace the couplings $u_{q'}, u_q$ under the integral by an average over the window $[-V/2, V/2]$ that is responsible for transport,

$$u_t(B) \stackrel{\text{def}}{=} \frac{1}{V}\int_{-V/2}^{V/2} d\epsilon_q u_q(B). \tag{58}$$

The integrals over $d\epsilon_{q'}$ and $d\epsilon_q$ can then be performed in closed form and one arrives at the following differential equation:

$$\frac{du_p}{dB} == \frac{u_p^2(B)}{2B}\left(\frac{1}{1+r}e^{-2B(-\epsilon_p - V/2)^2} + \frac{1}{1+r^{-1}}e^{-2B(-\epsilon_p + V/2)^2}\right) - \frac{u_t(B)}{4B^2}\int_0^B dB'\, u_p(B') u_t(B')\left(\frac{r + r^{-1}}{(1+r)(1+r^{-1})} + \frac{1}{(1+r)(1+r^{-1})}(2e^{-2BV^2} + \sqrt{2\pi}BV \operatorname{erf}(\sqrt{2}BV))\right). \tag{59}$$

We first use this to derive a closed equation for $u_t(B)$ from (58) by averaging over p:

$$\frac{du_t}{dB} = \frac{u_t^2(B)}{2B}\frac{\sqrt{\pi}}{\sqrt{8}BV}\operatorname{erf}(\sqrt{2}BV) - \frac{u_t(B)}{4B^2}\int_0^B dB'\, u_t^2(B') \times \left(\frac{r + r^{-1}}{(1+r)(1+r^{-1})} + \frac{1}{(1+r)(1+r^{-1})}(2e^{-2BV^2} + \sqrt{2\pi}BV \operatorname{erf}(\sqrt{2}BV))\right) \tag{60}$$

Of particular importance are also the running coupling constants at the left and right Fermi surfaces

$$u_l(B) \stackrel{\text{def}}{=} u_{\epsilon_p = V/2}(B), \quad u_r(B) \stackrel{\text{def}}{=} u_{\epsilon_p = -V/2}(B), \tag{61}$$

which will turn out to be relevant for the behavior of the quasiparticle resonances (Kondo peaks) and which determine the phase diagram since they correspond to extremal values of $u_p(B = \infty)$ as a function of B (see Section 4.5). Their flow equations follow immediately from (59):

$$\frac{du_l}{dB} = \frac{u_l^2(B)}{2B}\left(\frac{1}{1+r^{-1}} + \frac{1}{1+r}e^{-2BV^2}\right) - \frac{u_t(B)}{4B^2}\int_0^B dB'\, u_l(B') u_t(B') \times \left(\frac{r + r^{-1}}{(1+r)(1+r^{-1})} + \frac{1}{(1+r)(1+r^{-1})}(2e^{-2BV^2} + \sqrt{2\pi}BV \operatorname{erf}(\sqrt{2}BV))\right), \tag{62}$$

$$\frac{du_r}{dB} = \frac{u_r^2(B)}{2B}\left(\frac{1}{1+r} + \frac{1}{1+r^{-1}}e^{-2BV^2}\right) - \frac{u_t(B)}{4B^2}\int_0^B dB'\, u_r(B') u_t(B') \times \left(\frac{r + r^{-1}}{(1+r)(1+r^{-1})} + \frac{1}{(1+r)(1+r^{-1})}(2e^{-2BV^2} + \sqrt{2\pi}BV \operatorname{erf}(\sqrt{2}BV))\right). \tag{63}$$

The three differential equations (60), (62) and (63) are one of the key results of this work and allow us to describe and understand the scaling behavior of the non-equilibrium Kondo model [39].

4.2. Scaling analysis

We will first analyze (60), (62) and (63) in the initial phase of the flow where $\Lambda_{\text{feq}} \gg V$. As expected, all three differential equations coincide and one finds for $a = l, r, t$:

$$\frac{du_a}{d\Lambda_{\rm feq}} = -\frac{u_a^2}{\Lambda_{\rm feq}} + \frac{u_a^3}{2\Lambda_{\rm feq}} + \frac{O(u_a^4)}{\Lambda_{\rm feq}}. \tag{64}$$

Here we have used the approximation $\int_0^B dB' u_a^2(B') = B u_a^2(B)$, which holds plus correction terms in higher order due to the slow logarithmic flow of $u_a(B)$. The initial behavior of the running coupling constants is therefore determined by the equilibrium β-function (46) as expected. With our initial condition $u(B=0) = g_l + g_r$ this also agrees exactly with the scaling equations (4) from the analysis of Kaminski et al. [18] (with the identification $\Lambda_{\rm RG} = \Lambda_{\rm feq}$).

Once the flow parameter is smaller than the voltage bias, $\Lambda_{\rm feq} \ll V$, the scaling equations take a different structure. The effective transport coupling obeys

$$\frac{du_t}{d\Lambda_{\rm feq}} = u_t^3 \frac{V}{\Lambda_{\rm feq}^2} \sqrt{\frac{\pi}{2}} \frac{1}{(1+r)(1+r^{-1})}, \tag{65}$$

and the couplings at the left and right Fermi surfaces, resp.,

$$\frac{du_l}{d\Lambda_{\rm feq}} = -\frac{1}{1+r^{-1}} \frac{u_l^2}{\Lambda_{\rm feq}} + u_l u_t^2 \frac{V}{\Lambda_{\rm feq}^2} \sqrt{\frac{\pi}{2}} \frac{1}{(1+r)(1+r^{-1})}, \tag{66}$$

$$\frac{du_r}{d\Lambda_{\rm feq}} = -\frac{1}{1+r} \frac{u_r^2}{\Lambda_{\rm feq}} + u_r u_t^2 \frac{V}{\Lambda_{\rm feq}^2} \sqrt{\frac{\pi}{2}} \frac{1}{(1+r)(1+r^{-1})}. \tag{67}$$

One notices that the strong-coupling growth of the average transport coupling u_t stops when $\Lambda_{\rm feq} \sim V$ due to the energy difference of the left and right Fermi surfaces. On the other hand, the couplings at the left and right Fermi surfaces, u_l and u_r, still exhibit the typical Kondoesque strong-coupling behavior in quadratic order on the rhs of (66) and (67). This reflects the inter-lead scattering processes from the left lead back into the left lead, or likewise for the right lead: such processes still see a sharp Fermi surface for all $\Lambda_{\rm feq} < V$. It is this observation that has led to the prediction of 2-channel Kondo physics in the Kondo model with voltage bias based on a 1-loop calculation [28].

However, different from the experience in equilibrium models the third order terms in (66) and (67) can become more important than the second-order terms even for small coupling constants: this is due to the more strongly growing $V/\Lambda_{\rm feq}^2$ terms as compared to the conventional $1/\Lambda_{\rm feq}$ behavior in quadratic order in the infrared limit $\Lambda_{\rm feq} \to 0$. Since the third-order term has a positive sign, it counteracts the second-order term and can avoid the strong-coupling divergence. Figs. 3 and 4 show the numerical solution of (60), (62) and (63) for symmetric ($r = 1$) and asymmetric Kondo dots ($r = 2$). One can see that indeed all couplings remain finite for sufficiently large voltage bias which shows that there is no 2-channel strong-coupling divergence.

Before proceeding with analyzing the resulting phase diagram in more detail, we will first get some more analytical insights into the solution of the scaling equations. The solution of (65) is straightforward

$$u_t(\Lambda_{\rm feq}) = \frac{u_*}{\sqrt{1 + \Gamma_{\rm rel}/\Lambda_{\rm feq}}}. \tag{68}$$

Here,

$$\Gamma_{\rm rel} \stackrel{\rm def}{=} \sqrt{2\pi} u_*^2 V \frac{1}{(1+r)(1+r^{-1})}, \tag{69}$$

where u_* is the running coupling constant on the scale $\Lambda_{\rm feq} = V$ (since we can safely neglect $\Gamma_{\rm rel}/V$ in the weak-coupling regime). From the solution of (64), we then find

$$u_* = u(\Lambda_{\rm feq} = V) = \frac{1}{\ln(V/T_{\rm K})} \tag{70}$$

with the Kondo temperature defined from the equilibrium model

$$T_{\rm K} = D\sqrt{g_l + g_r} e^{-1/(g_l+g_r)}. \tag{71}$$

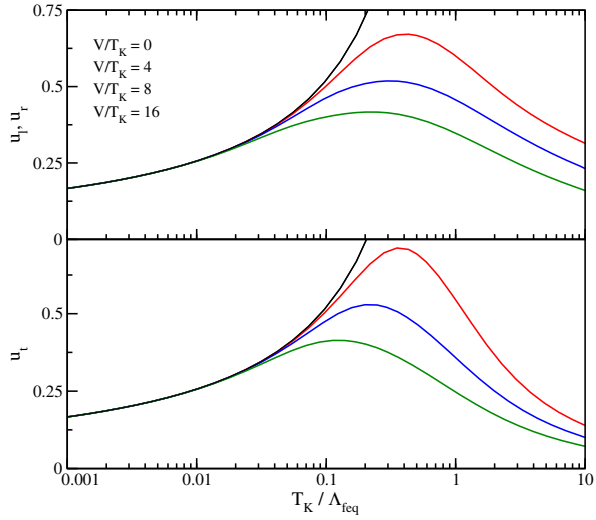

Fig. 3. Universal curves for the flow of u_l (equal to u_r) and u_t for symmetric Kondo dots ($r = 1$). Results are shown for various ratios V/T_K labelling the curves from top to bottom.

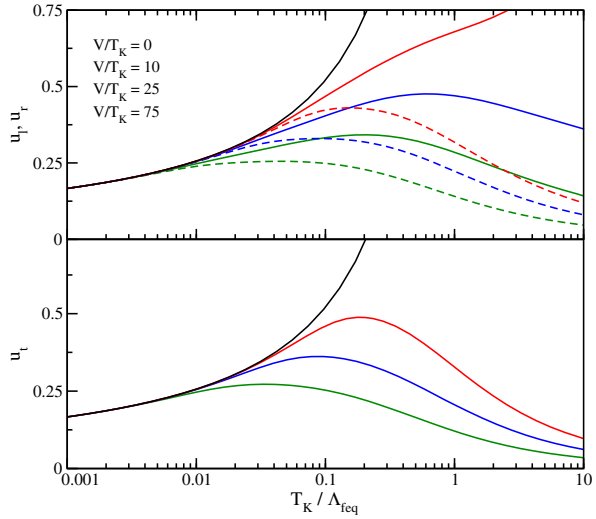

Fig. 4. Universal curves for the flow of u_l (full lines), u_r (dashed lines) and u_t for asymmetrically coupled Kondo dots with $r = \Gamma_l/\Gamma_r = 2$. Results are shown for various ratios V/T_K labelling the curves from top to bottom. Notice that u_l and u_r coincide for $V = 0$, therefore only u_l is shown.

In order to understand the implication of the flow of u_t on u_l and u_r it is convenient to first rewrite (66) and (67) in the following equivalent form:

$$\frac{du_l}{d\ln \Lambda_{\text{feq}}} = -\frac{u_l^2}{1+r^{-1}} + u_l \frac{d\ln u_t}{d\ln \Lambda_{\text{feq}}}, \tag{72}$$

$$\frac{du_r}{d\ln \Lambda_{\text{feq}}} = -\frac{u_r^2}{1+r} + u_r \frac{d\ln u_t}{d\ln \Lambda_{\text{feq}}}. \tag{73}$$

Since

$$\frac{d\ln u_t}{d\ln \Lambda_{\rm feq}} = \frac{1}{2}\frac{\Gamma_{\rm rel}}{\Lambda_{\rm feq}+\Gamma_{\rm rel}}, \tag{74}$$

this implies

$$\frac{du_l}{d\ln \Lambda_{\rm feq}} = u_l\left(-\frac{u_l}{1+r^{-1}}+\frac{1}{2}\frac{\Gamma_{\rm rel}}{\Lambda_{\rm feq}+\Gamma_{\rm rel}}\right), \tag{75}$$

$$\frac{du_r}{d\ln \Lambda_{\rm feq}} = u_r\left(-\frac{u_r}{1+r}+\frac{1}{2}\frac{\Gamma_{\rm rel}}{\Lambda_{\rm feq}+\Gamma_{\rm rel}}\right). \tag{76}$$

These equations show a remarkable *transmutation* of the third-order terms in the running coupling constant into linear terms once $\Lambda_{\rm feq} \lesssim \Gamma_{\rm rel}$. This transmutation is possible due to the $\Lambda_{\rm feq}^{-2}$-terms in (66) and (67) (or, equivalently, due to the $B^{-1/2}$-terms in (62) and (63) as opposed to the equilibrium B^{-1}-terms). For $\Lambda_{\rm feq} \gg \Gamma_{\rm rel}$, these linear order terms are negligible and u_l, u_r exhibit typical Kondo-esque strong-coupling scaling. In the later phase of the flow, the couplings become small again with $u_l(\Lambda_{\rm feq}), u_r(\Lambda_{\rm feq}) \propto \Lambda_{\rm feq}^{1/2}$ if they are not already too large on the scale $\Gamma_{\rm rel}$.

Let us analyze the meaning of this scale $\Gamma_{\rm rel}$. We have already quoted the result from Kaminski et al. [18] that for $V \gg T_{\rm K}$ the current I is to leading order given by (9)

$$I = \frac{e^2}{h}\frac{3\pi^2}{2}u_*^2 V \frac{1}{(1+r)(1+r^{-1})}. \tag{77}$$

From (69), we can see that $\Gamma_{\rm rel} \propto I$ with a proportionality factor independent of V, $T_{\rm K}$ and r. It is therefore natural to associate $\Gamma_{\rm rel}$ with the spin decoherence rate generated by the shot noise proportional to the current. The third-order terms in the scaling equations therefore describe spin decoherence due to the non-equilibrium current that cuts off the strong-coupling behavior of the inter-lead scattering processes. This observation in our Hamiltonian scaling framework is in agreement with the work by Rosch et al. [20] that such non-equilibrium decoherence processes eliminate the 2-channel strong-coupling divergence in the non-equilibrium Kondo model with $J_{lr}^2 = J_{ll}J_{rr}$.

We will next use the flow equation analysis to study quantitatively the interplay between coherent (equilibrium) strong-coupling processes and decoherence generated by the non-equilibrium current in a systematic expansion in terms of renormalized parameters. Before proceeding along these lines, it is worthwhile to point out that decoherence acts differently from temperature in the Kondo scaling equations: decoherence and strong-coupling physics are in competition in (75) and (76), whereas non-zero temperature T already eliminates the strong-coupling term itself, e.g.

$$\frac{dg}{d\ln \Lambda} = -g^2 e^{-T/\Lambda} \tag{78}$$

for the equilibrium Kondo model (37) in both the conventional scaling and the flow equation approach. We would also like to mention the important question of how one can understand within the flow equation framework that the third-order terms in the scaling equations are really associated with *spin decoherence*. We will postpone the answer to this question to the discussion of the dynamic spin correlation function later in Section 5.3, where we will work out this correspondence in detail.

4.3. Weak- and strong-coupling regime

From the scaling equation for u_l, u_r and u_t, we can now determine the scaling behavior of the non-equilibrium Kondo model: that is we determine the regions in the parameter space where all coupling constants remain small (weak-coupling regime) or where at least one the coupling constants becomes large (strong-coupling regime). Since only u_l and u_r can continue to grow below $\Lambda_{\rm feq} \approx V$ according to (75) and (76) (as opposed to u_t), these regions are determined by the behavior of u_l for $r = \Gamma_l/\Gamma_r > 1$, or by the behavior of u_r for $r < 1$. Because of the trivial exchange symmetry $r \leftrightarrow r^{-1}$, we can focus on $r \geqslant 1$ below without loss of generality.

From (75), we can deduce an (approximate) condition for $u_l(\Lambda_{\rm feq})$ remaining small during the entire flow

$$\frac{u_l(\Gamma_{\rm rel})}{1+r^{-1}} \lesssim \frac{1}{2}. \tag{79}$$

In the notation of the original Kondo Hamiltonian (1), this is equivalent to the inter-lead scattering processes being not too large on the scale $\Gamma_{\rm rel}$:

$$\rho J_{ll} \lesssim \frac{1}{2}. \tag{80}$$

We can approximately rewrite this condition in terms of renormalized quantities by explicitly integrating up the quadratic part of (66). One finds

$$\frac{u_l(\Gamma_{\rm rel})}{1+r^{-1}} = \frac{1}{\ln\left(\frac{V}{T_{\rm K}}\right)^{1+r^{-1}} + \ln\left(\frac{\Gamma_{\rm rel}}{V}\right)} \tag{81}$$

leading to

$$\left(\frac{V}{T_{\rm K}}\right)^{1+r^{-1}} \frac{\sqrt{2\pi}}{\ln^2(V/T_{\rm K})} \frac{1}{(1+r)(1+r^{-1})} \gtrsim e^2. \tag{82}$$

Comparison with the numerical solution below shows that (82) can be used as an approximate condition for the weak-coupling regime for $r \gtrsim 2$. Before proceeding with the numerical solution of the full differential equation for u_l, one can deduce some important analytical insights from (82): the "critical" value of the voltage bias $V/T_{\rm K}$ increases for increasing values of the asymmetry r. For larger values of r, this is due to the fact that decoherence is proportional to the current, which is suppressed for asymmetric coupling to the leads: $I/T_{\rm K}$ is maximum for $r = 1$. The third term on the lhs of (82) thus reflects the r-dependence of the unitarity limit of the conductance G_u in (10).

The above (approximate) analytical results are confirmed by the exact numerical solution of the full differential equations (62), (63) and (60) for the running couplings u_l, u_r and u_t. The definition of "strong-coupling regime" versus "weak-coupling regime" is necessarily not unique since we expect a smooth crossover between these regimes. The definition used in our analysis is that in the weak-coupling regime the couplings u_l and u_r remain smaller than 0.75 during the entire flow, whereas in the strong-coupling regime at least one these coupling becomes larger than 0.75. Choosing a somehow different value than 0.75 (e.g. using 0.5 or 1.0 instead) does actually hardly change the crossover line. The actual value of 0.75 is motivated by the observation that then the T-matrix reaches the unitarity limit at the resp. Fermi surface in renormalized second-order perturbation theory. This indicates the breakdown of our perturbative expansion in the running coupling constant and therefore limits the region where our method is reliable. The numerical results for this crossover line between strong-coupling and weak-coupling regime are depicted in Fig. 5.

Fig. 5 shows that the strong-coupling regime extends to remarkably large values of the voltage bias for asymmetric Kondo dots (as we have already qualitatively deduced from (82)). By comparison with the flow diagrams in Figs. 3 and 4, we can see that while there is no 2-channel Kondo physics (in the sense of a 2-channel strong-coupling divergence), the crossover to the strong-coupling regime is essentially given by 1-channel Kondo physics for asymmetric Kondo dots: the couplings at the more strongly coupled Fermi surface dominate the Kondo impurity physics.

It should be emphasized again that one expects a smooth crossover between weak-coupling and strong-coupling regimes. While this issue cannot be definitely answered using the weak-coupling tools here, there is no physical reason to expect anything else than a smooth crossover. Notice that for the equilibrium Kondo model at finite temperature we do know that there is a smooth crossover between weak- and strong-coupling regimes. In this context, the question arises what physical properties actually distinguish the strong-coupling regime from the weak-coupling regime. We will address this question in detail later when we discuss the behavior of observables: suitable observables behave quantitatively different in these regimes and make the weak-coupling vs.

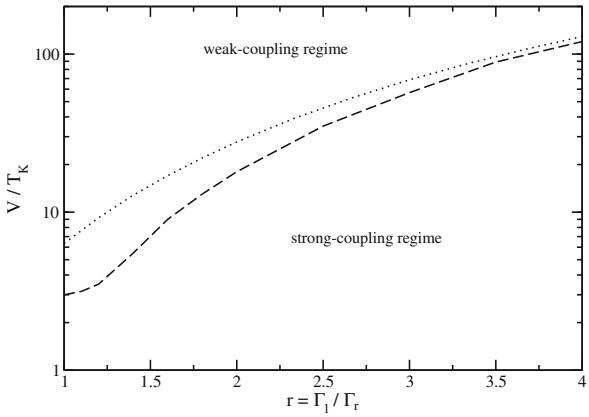

Fig. 5. Scaling picture of the non-equilibrium Kondo model as a function of asymmetry $r = \Gamma_l/\Gamma_r$ and voltage bias. The dashed line separates the weak-coupling regime from the strong-coupling regime (deduced from the full numerical solution, see text). The dotted line is the approximate analytical result (82).

strong-coupling distinction both useful and relevant for the interpretation of experiments. For example in the strong-coupling regime, the local density of states remains nearly pinned to its Friedel value at the more strongly coupled Fermi surface, and it only decays once the voltage bias is well into the weak-coupling regime.

4.4. Expansion schemes and higher orders

We have already mentioned the remarkable *transmutation* of a third-order term in the running coupling constant into a linear term, compare e.g. (66) and (75) for $u_l(\Lambda_{\rm feq})$. Decoherence therefore essentially makes the running coupling irrelevant with a canonical scaling dimension +1/2 for $\Lambda_{\rm feq} \lesssim \Gamma_{\rm rel}$. This teaches an important lesson regarding the well-established notion that higher-order terms in the running coupling constant cannot change the results of lower order calculations qualitatively if the running coupling constant remains sufficiently small during the flow (i.e., in the weak-coupling regime). It was exactly this observation which eliminated the possibility of 2-channel Kondo physics due to diverging inter-lead scattering processes.

The technical reason for the transmutation in our non-equilibrium model is the existence of the dimensionful parameter voltage bias V, which allows terms like $V/\Lambda_{\rm feq}^2$ alongside the conventional $1/\Lambda_{\rm feq}$-terms in the scaling equations (65)–(67). Therefore, the possibility of such a transmutation always arises whenever we have dimensionful parameter in a scaling problem, which should be of importance also for analyzing other problems and interpreting the results of lower order calculations. The unavoidable general conclusion is that the expansion order by order in the running coupling constant is not a systematic expansion anymore, unless we can show that no such "transmutation" occurs and changes the results. Notice that for example the equilibrium Kondo model at finite temperature contains the dimensionful parameter temperature T, which in fact also leads to transmutation in its third-order terms.[38] However, already the second-order term loses its strong-coupling behavior at sufficiently large temperature according to (78), and therefore no qualitative changes occur due to the third-order terms.

It is worthwhile to mention again the conceptual difference between the flow equation framework and the conventional scaling analysis around the two Fermi surfaces, compare Fig. 1. For $\Lambda_{\rm RG} \ll V$ the scaled Hamiltonian has no "knowledge" of the energy scale voltage bias anymore and therefore cannot generate the $V/\Lambda_{\rm RG}^2$-terms in third order (2-loop order). On the other hand, the flow equation Hamiltonian still contains all sufficiently energy-diagonal scattering processes for $\Lambda_{\rm feq} \ll V$ (compare Fig. 2), and therefore "knows" about the energy voltage bias because this is the energy window where scattering processes contributing to the current are possible between the left and the right lead. It is exactly this observation which leads to the $V/\Lambda_{\rm feq}^2$-terms in the flow equation scaling equations.

In this context, one should also address the effect of higher-order terms in the flow equation scaling equations. One can verify that the most IR-singular behavior in fourth order is $u^4 V/\Lambda_{\mathrm{feq}}^2$, which is therefore smaller than the third-order terms in (65)–(67) in the weak-coupling regime. In fifth order, it seems possible to have contributions that modify the $\sqrt{2\pi}$-proportionality factor in our result for the relaxation rate (69), however, they cannot change the structure of (75) or (76). More quantitative results would be a formidable task equivalent to a 4-loop calculation. These observations indicate that the third-order calculation presented here should give reliable quantitative results in the entire non-equilibrium weak-coupling regime.

4.5. Numerical solution

In the previous sections, we have obtained analytical insights into the competition of decoherence and strong-coupling behavior in the non-equilibrium Kondo model. In order to do this, we have used various approximations starting from the full set of flow equations (52) and (53). More accurate results, which also allow us to check the accuracy of the approximations leading to (65)–(67), can be obtained by solving the full systems of differential equations. These solutions will also be important for obtaining quantitative results for the behavior of dynamical quantities later in Section 5. The numerical effort for solving (52) and (53) scales with N^2, where N is the number of band states taken into account for the numerical solution: details of the implementation of the numerics are contained in Appendix A.3.

Figs. 6 and 7 depict the flow of the coupling constants $u_p(\Lambda_{\mathrm{feq}}) = \rho J_{pp}(\Lambda_{\mathrm{feq}})$ for a symmetric and an asymmetric Kondo dot in the weak-coupling regime. One observes the buildup of strong-coupling behavior at the left and right Fermi surface, followed by decoherence effects that lead to a decay of the coupling constants. In Fig. 7, one can also notice the asymmetry in the buildup of the resonances at the two Fermi surfaces due to the stronger effect of decoherence at the more weakly coupled lead.

Figs. 8 and 9 shows a comparison of the flow of the coupling constants $u_l(\Lambda_{\mathrm{feq}}), u_r(\Lambda_{\mathrm{feq}})$ and $u_t(\Lambda_{\mathrm{feq}})$ from the full numerical solution with the solution of (60), (62) and (63). One can see that our approximations in going from $N \times N$ differential equations to just three differential equations were very accurate: the resp. solutions agree very well. This agreement is somehow obvious in the initial phase of the flow where the voltage bias plays no role. Therefore, one can safely start the full numerical solution at

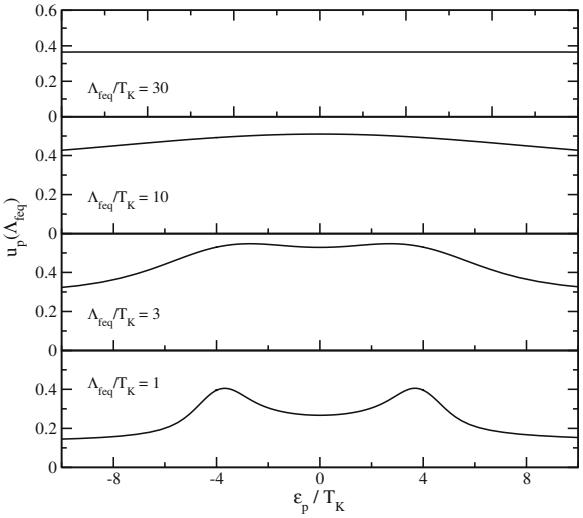

Fig. 6. Running coupling constants $u_p(\Lambda_{\mathrm{feq}})$ at various points during the flow for a symmetric Kondo dot with $V/T_{\mathrm{K}} = 8.0$. One observes the initial buildup of strong-coupling behavior until $\Lambda_{\mathrm{feq}}/T_{\mathrm{K}} \approx 3$, followed by decreasing coupling constants even at the left and right Fermi surfaces due to decoherence: there is no 2-channel strong-coupling divergence.

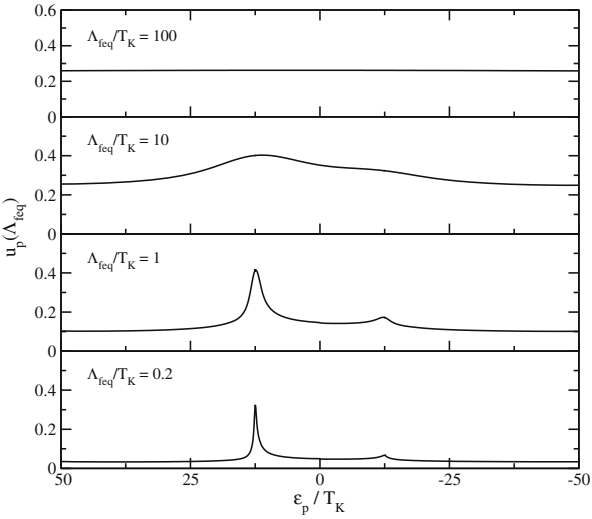

Fig. 7. Running coupling constants $u_p(\Lambda_{\text{feq}})$ at various points during the flow for an asymmetric Kondo dot with $r = \Gamma_l/\Gamma_r = 2$ and $V/T_K = 25.0$. One observes a much stronger buildup of strong-coupling behavior at the more strongly coupled lead (Fermi surface at $\epsilon_p = 12.5T_K$).

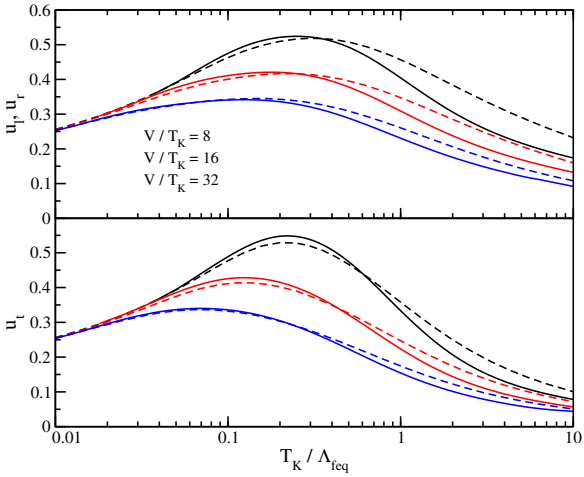

Fig. 8. Comparison of the flow of the coupling constants u_l and u_t from the full numerical solution of (52) and (53) with the effective Eqs. (60) and (62). Depicted here is a symmetric Kondo dot (therefore $u_l = u_r$). The full lines refer to the full numerical solution and the dashed lines to the effective equations. Results are shown for various ratios V/T_K labelling the pairs of curves from top to bottom.

$\Lambda_{\text{feq}} = 4\,V$ and not waste computer time with larger values of the initial cutoff. The curves agree very well until one reaches the decoherence scale (maximum of the coupling constants), which was important for determining the phase diagram. The small absolute differences at the decoherence scale between the full numerical solution and the analytical approximation get somehow amplified if one looks at the relative error in the later phase of the flow. This will, however, anyway turn out to be unimportant for the evaluation of observables (which are essentially determined by the absolute values of the coupling constants at the decoherence scale). In general, one can notice from Figs. 8 and 9 that the accuracy of our analytical approximations (60), (62) and (63) becomes increasingly better if the coupling constants remain small during the flow, that is for larger values of the voltage bias V/T_K.

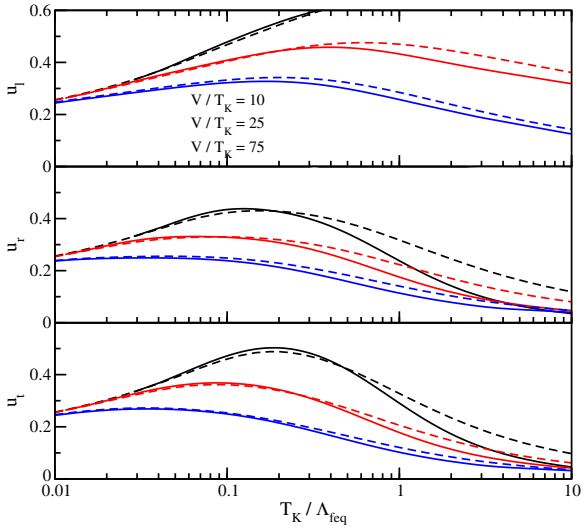

Fig. 9. Same as Fig. 8 for the flow of u_l, u_r and u_t for an asymmetric Kondo dot with $r = \Gamma_l/\Gamma_r = 2$. The curves for $V/T_K = 10$ should only be considered until $T_K/\Lambda_{feq} \approx 0.3$ since the scaling flow leaves the weak-coupling regime for smaller flow parameters Λ_{feq}.

These observations therefore justify a posteriori our previous analytical analysis based on (60), (62) and (63).

5. Observables

5.1. Observables in the flow equation framework

The evaluation of dynamical quantities like correlation functions within the flow equation framework is rather different from conventional many-body techniques. The key observation is that while the time evolution becomes trivial in the diagonal basis for $B \to \infty$, the structure of observables can be very complicated in this basis [24]. In order to use the time evolution with respect to the diagonal Hamiltonian $H(B = \infty)$, one first needs to transform an observable O with the same unitary transformations as the Hamiltonian itself (12)

$$\frac{dO(B)}{dB} = [\eta(B), O(B)], \tag{83}$$

where $O(B = 0) = O$ is the operator in the original basis. Once has found $O(B = \infty)$, it becomes easy to work out its equilibrium correlation functions: we are for example interested in

$$C_{eq}(t) = \langle GS|O(t)O(0)|GS\rangle = \langle GS|e^{iHt}Oe^{-iHt}O|GS\rangle, \tag{84}$$

where $|\,GS\rangle$ is the interacting ground state of the system. We denote the unitary transformation that connects the initial with the final basis with $U(B = \infty)$, therefore

$$\widetilde{H} = H(B = \infty) = U(B = \infty)H(B = 0)U^\dagger(B = \infty),$$
$$\widetilde{O} = O(B = \infty) = U(B = \infty)O(B = 0)U^\dagger(B = \infty),$$

where we have introduced the notation $\sim$ that designates an operator in the transformed basis. One can (at least formally) construct $U(B = \infty)$ from (12) in the following way:

$$U(B) \stackrel{\text{def}}{=} T_B \exp\left(\int_0^B dB'\,\eta(B')\right). \tag{85}$$

Here, T_B denotes B-ordering in the same way as the usual time-ordering: the generator $\eta(B_i')$ with the largest B_i' is commuted all the way to the left, next comes the second largest, etc. Next one inserts identities $U^\dagger(B=\infty)U(B=\infty)=1$ everywhere in (84) and arrives at

$$C_{\mathrm{eq}}(t) = \langle \mathrm{GS}|U^\dagger(B=\infty)e^{\widetilde{iHt}}\widetilde{O}e^{-\widetilde{iHt}}\widetilde{O}U(B=\infty)|\mathrm{GS}\rangle. \tag{86}$$

A key observation is that $U(B=\infty)\mid \mathrm{GS}\rangle$ is just the ground state of the diagonal Hamiltonian $\widetilde{H}$, which is therefore trivial to write down (depending on the system for example just the vacuum, the non-interacting Fermi sea, etc.)

$$|\mathrm{GS}_{\widetilde{H}}\rangle = U(B=\infty)|\mathrm{GS}\rangle. \tag{87}$$

The evaluation of equilibrium correlation functions therefore reduces to

$$C_{\mathrm{eq}}(t) = \langle \mathrm{GS}_{\widetilde{H}}|e^{\widetilde{iHt}}\widetilde{O}e^{-\widetilde{iHt}}\widetilde{O}|\mathrm{GS}_{\widetilde{H}}\rangle. \tag{88}$$

Since it is usually straightforward to solve the Heisenberg equations of motion for an operator with respect to the diagonal Hamiltonian $\widetilde{H}$, this equation has been used as the starting point for the evaluation of correlation functions in various models like the spin-boson model [29,30], the Kondo model [26], etc. Before proceeding along the same lines, we first need to reconsider the changes in this derivation for a non-equilibrium model like the Kondo model with voltage bias.

The fundamental difference from the equilibrium situation is that now we are *not* interested in evaluating observables in the ground state. Rather, the relevant question is the behavior of observables in the *steady state* that evolves after switching on the coupling between the left and right lead and then waiting long enough. This is also the key idea of the Keldysh approach and in this manner one circumvents the generally unanswered fundamental question on how to construct a non-equilibrium steady state. We follow the same idea here by replacing (84) with its non-equilibrium generalization

$$C_{\mathrm{neq}}(t) \stackrel{\mathrm{def}}{=} \lim_{t_w\to\infty} C(t,t_w), \tag{89}$$

where

$$C(t,t_w) \stackrel{\mathrm{def}}{=} \langle \Psi_i|O(t+t_w)O(t_w)|\Psi_i\rangle = \langle \Psi_i|e^{iH(t+t_w)}Oe^{-iH(t+t_w)}e^{iHt_w}Oe^{-iHt_w}|\Psi_i\rangle. \tag{90}$$

Here, we assume that the thermodynamic limit is always taken before sending the waiting time t_w for the measurement to infinity in (89). Notice that in general $C_{\mathrm{neq}}(t)$ could depend on the initial state $\mid \Psi_i\rangle$ and in the sequel we will use an initial state that is directly related to the experimental situation: $\mid \Psi_i\rangle$ is the ground state of the system when the two leads are not coupled via the Kondo impurity, that is the non-interacting Fermi sea in both the left and right lead separately.

We now use the same unitary transformations as going from (84) to (86)

$$C(t,t_w) = \langle \Psi_i|U^\dagger(B=\infty)e^{\widetilde{iH(t+t_w)}}\widetilde{O}e^{-\widetilde{iH(t+t_w)}}U(B=\infty)U^\dagger(B=\infty)e^{\widetilde{iHt_w}}\widetilde{O}e^{-\widetilde{iHt_w}}U(B=\infty)|\Psi_i\rangle. \tag{91}$$

The additional unitary transformation of the time-evolved operator in the diagonal basis just maps back to the original basis, where the initial state is specified. This *forward-backward scheme* has also been employed in other models [8] where one is interested in real-time evolution from some given initial state. The backward transformation part of this scheme can be implemented by solving (83) from $B=\infty$ to $B=0$: the initial condition at $B=\infty$ is just the time-evolved operator in the diagonal basis. In order to evaluate (89) from this expression, we next need to say something about the explicit transformation behavior of the spin operator in the following section.

5.2. Transformation of the spin operator

The transformation of the spin operator $\vec{S}$ under the flow equation transformation has already been worked out in [24] and we only give the key steps here. One makes the following ansatz for the flowing observable (83):

$$\vec{S}(B) = h(B)\vec{S} + i\sum_{p',p}\gamma_{p'p}(B)\vec{S}\times\vec{s}_{p'p} + O(u^2) \tag{92}$$

and derives the flow equations for the coefficients from (83):

$$\begin{aligned}\frac{dh}{dB} &= \sum_{p',p}(\epsilon_{p'}-\epsilon_p)J_{p'p}\gamma_{pp'}n_f(p')(1-n_f(p)),\\ \frac{d\gamma_{p'p}}{dB} &= h(\epsilon_{p'}-\epsilon_p)J_{p'p} - \frac{1}{4}\sum_u((\epsilon_{p'}-\epsilon_u)J_{p'u}\gamma_{up} + (\epsilon_p-\epsilon_u)J_{up}\gamma_{p'u})(1-2n_f(u)).\end{aligned} \tag{93}$$

Initially $h(B=0)=1$, $\gamma_{p'p}(B=0)=0$ and under the flow one always finds $h(B=\infty)=0$ (see [24,29]). One easily identifies this scale where $h(B)$ rapidly drops to 0 by noticing that $\gamma_{p'p}(B)$ is initially only generated in order u, therefore $h(B)$ initially remains nearly constant since its differential equation only generates terms in order u^2. This picture breaks down on the scale $\Lambda_{\mathrm{feq}}\sim\Gamma_{\mathrm{rel}}$ where $h(B)$ starts to decay algebraically $\propto B^{-1/4}$:

(i) Non-equilibrium (voltage bias V):

$$\Gamma_{\mathrm{rel}}(V) = \sqrt{2\pi}u^2(\Lambda_{\mathrm{feq}}=V)\frac{V}{(1+r)(1+r^{-1})}. \tag{94}$$

(ii) Equilibrium (non-zero temperature):

$$\Gamma_{\mathrm{rel}}(T) = \sqrt{2\pi}u^2(\Lambda_{\mathrm{feq}}=T)T. \tag{95}$$

Notice that these energy scales are identical with the flow scale (69) where the transmutation of the third-order terms in the coupling constant into linear terms occurs. At this point, it is easy to understand this observation: When $h(B)$ becomes small, the spin operator (92) completely decays into its entangled form $\vec{S}\times\vec{s}_{p'p}$. In the flow of the Hamiltonian, this amounts to transforming the marginally relevant interaction term $J_{t't}\vec{S}\cdot s_{t't}$ into the irrelevant K-term, $K_{t't,p'p}\vec{S}\cdot(\vec{s}_{t't}\times\vec{s}_{p'p})$. This implies that the flow equations for u_t, u_l, u_r (74)–(76) become weak-coupling for $\Lambda_{\mathrm{feq}}\lesssim\Gamma_{\mathrm{rel}}$ as discussed before. In the next section, we will identify the energy scale where the decoherence effects become important in the Hamiltonian flow with the width of the zero frequency peak of the correlation function, that is the physical relaxation rate.

5.3. Dynamical spin response and correlation functions

In the following, we will use the shorthand $\tilde{\gamma}_{p'p}$ for $\gamma_{p'p}(B=\infty)$. From (88), one derives the following expression for the symmetrized spin–spin correlation function in equilibrium at non-zero temperature:

$$\begin{aligned}C_{\mathrm{eq}}(t) \stackrel{\mathrm{def}}{=} \frac{1}{2}\langle\{S_z(0),S_z(t)\}\rangle &= -\frac{1}{2}\sum_{p',p}\sum_{q',q}\tilde{\gamma}_{p'p}\tilde{\gamma}_{q'q}e^{i(\epsilon_{q'}-\epsilon_q)t}\langle\mathrm{FS}|\{(\vec{S}\times\vec{s}_{p'p})^z,(\vec{S}\times\vec{s}_{q'q})^z\}|\mathrm{FS}\rangle\\ &= \frac{1}{8}\sum_{p',p}\tilde{\gamma}_{p'p}^2e^{i(\epsilon_{p'}-\epsilon_p)t}(n_f(p)(1-n_f(p')) + n_f(p')(1-n_f(p))).\end{aligned} \tag{96}$$

Here, $|\,\mathrm{FS}\rangle$ is the non-interacting Fermi sea and $n_f(p)$ the finite temperature Fermi–Dirac distribution.

For the symmetrized spin–spin correlation function in the non-equilibrium steady state (89), we need to perform the backtransformation (91) of $\widetilde{S}_z(t_w)$ for large t_w. Due to the phases $\exp[i(\epsilon_{q'}-\epsilon_q)t_w]$ that the matrix elements $\tilde{\gamma}_{q'q}$ acquire, one can easily see that integrating (93) back from $B=\infty$ to $B=0$ only leads to higher-order contributions in the flow equations. For large times, we can therefore say

$$S_z(t_w) = \widetilde{S}_z(t_w)(1+O(g)). \tag{97}$$

This implies for the spin–spin correlation function in the steady state (89)

$$C_{\text{neq}}(t) = \frac{1}{8}\sum_{p',p} \tilde{\gamma}^2_{p'p} e^{i(\epsilon_{p'}-\epsilon_p)t}(n_f(p)(1-n_f(p')) + n_f(p')(1-n_f(p))) \tag{98}$$

plus higher-order corrections in the running coupling constant. Here, we now have to insert the occupation numbers (55) for the problem with voltage bias.

Both the non-zero temperature equilibrium result (96) and the steady state non-equilibrium result (98) have the same structure and can therefore be analyzed together: Fourier transformation yields

$$C(\omega) = \int dt\, e^{i\omega t} C(t) = \frac{\pi}{4}\sum_p \tilde{\gamma}^2_{p+\omega,p}(n_f(p)(1-n_f(p+\omega)) + n_f(p+\omega)(1-n_f(p))), \tag{99}$$

where the notation $p+\omega$ stands for the state with energy $\epsilon_p + \omega$. Due to the perturbative nature of the transformation, the sum rule

$$\int_{-\infty}^{\infty} d\omega\, C(\omega) = 2\pi\langle S_z^2\rangle = \frac{\pi}{2} \tag{100}$$

is not fulfilled exactly. For high voltage bias or high temperature, this violation is typically only of order 1%, which becomes up to 10% for voltage bias or temperature of order T_K.

The same calculation for the spin susceptibility

$$\chi(t) \stackrel{\text{def}}{=} -i\Theta(t)\langle[S_z(t), S_z(0)]\rangle \tag{101}$$

yields the imaginary part of its Fourier transform

$$\chi''(\omega) = \frac{\pi}{4}\sum_p \tilde{\gamma}^2_{p+\omega,p}(n_f(p)(1-n_f(p+\omega)) - n_f(p+\omega)(1-n_f(p))). \tag{102}$$

The real part follows via a Kramers–Kronig relation, in particular the static spin susceptibility χ_0 is given by

$$\chi_0 = \frac{1}{\pi}\int_{-\infty}^{\infty} d\omega \frac{\chi''(\omega)}{\omega}. \tag{103}$$

Notice that the fluctuation–dissipation theorem [40]

$$\chi''(\omega) = \tanh\left(\frac{\omega}{2T}\right) C(\omega) \tag{104}$$

is fulfilled exactly in equilibrium. In non-equilibrium, the fluctuation–dissipation relation is fulfilled approximately in the zero frequency limit if one inserts an effective temperature motivated by the comparison of (94) and (95):

$$T_{\text{eff}} = \frac{V}{(1+r)(1+r^{-1})}. \tag{105}$$

Typical curves for the spin–spin correlation function and the imaginary part of the dynamical spin susceptibility are shown in Fig. 10 for non-equilibrium (for varying voltage bias) and in Fig. 11 for equilibrium (for varying temperature). The spin–spin correlation function is a symmetric function of ω with a zero frequency peak of width Γ_{rel}. The imaginary part of the dynamical spin susceptibility is an antisymmetric function of ω and has its maximum at $\chi''(\omega \approx \Gamma_{\text{rel}})$. An approximate analytical solution of (93) yields [24] (see also [20]):

$$C(\omega) \sim \begin{cases} \frac{1}{\Gamma_{\text{rel}}} & \text{for } |\omega| \lesssim \Gamma_{\text{rel}}, \\ \frac{\Gamma_{\text{rel}}}{\omega^2} & \text{for } \Gamma_{\text{rel}} \lesssim |\omega| \lesssim T_{\text{eff}}, \\ \frac{u^2(\Lambda_{\text{feq}}=|\omega|)}{|\omega|} & \text{for } T_{\text{eff}} \lesssim |\omega|, \end{cases} \tag{106}$$

$$\chi''(\omega) \sim \begin{cases} \frac{u^2(\Lambda_{\text{feq}}=T,V)}{\Gamma_{\text{rel}}^2}\omega & \text{for } |\omega| \lesssim \Gamma_{\text{rel}}, \\ \frac{u^2(\Lambda_{\text{feq}}=|\omega|)}{\omega} & \text{for } \Gamma_{\text{rel}} \lesssim |\omega|. \end{cases} \tag{107}$$

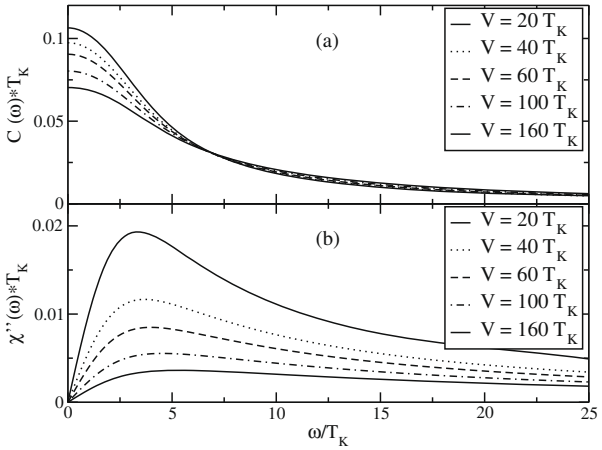

Fig. 10. Universal curves for (a) the spin–spin correlation function $C(\omega)$ and (b) the imaginary part of the dynamical spin susceptibility $\chi''(\omega)$ in non-equilibrium (symmetric coupling $r = 1$).

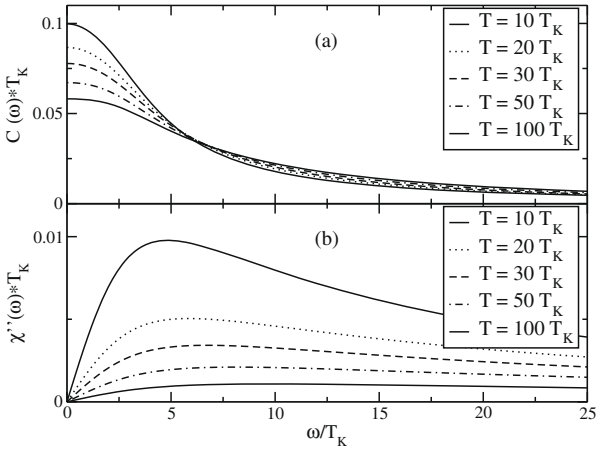

Fig. 11. Universal curves for (a) the spin–spin correlation function $C(\omega)$ and (b) the imaginary part of the dynamical spin susceptibility $\chi''(\omega)$ in equilibrium for various temperatures.

Notice that the zero frequency peak of the correlation function is directly related to the flow scale where $h(B)$ in the transformation of the spin operator starts to deviate noticeably from 1 since essentially all the spectral weight is contained in the energy interval $O(\Gamma_{\mathrm{rel}})$ according to (106). This provides the desired physical interpretation of Γ_{rel} defined in (69): the energy scale where the Kondo coupling becomes irrelevant can be identified with the spin relaxation rate.

In Fig. 12, we show the spin–spin correlation function and the imaginary part of the dynamical spin susceptibility for asymmetric coupling to the leads with $r = 2$. In Fig. 13, we depict the dependence on the asymmetry parameter r at fixed voltage bias. Increasing the asymmetry parameter r leads to a smaller decoherence rate since the effective temperature (105) becomes smaller. In agreement with (106) and (107), one therefore notices that mainly the low frequency properties are affected with the maxima of the curves increasing for larger asymmetry.

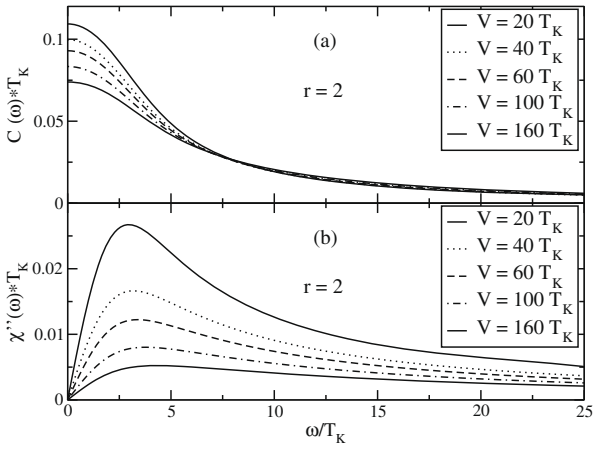

Fig. 12. Universal curves for (a) the spin–spin correlation function $C(\omega)$ and (b) the imaginary part of the dynamical spin susceptibility $\chi''(\omega)$ in non-equilibrium for asymmetric coupling of the leads $r = 2$.

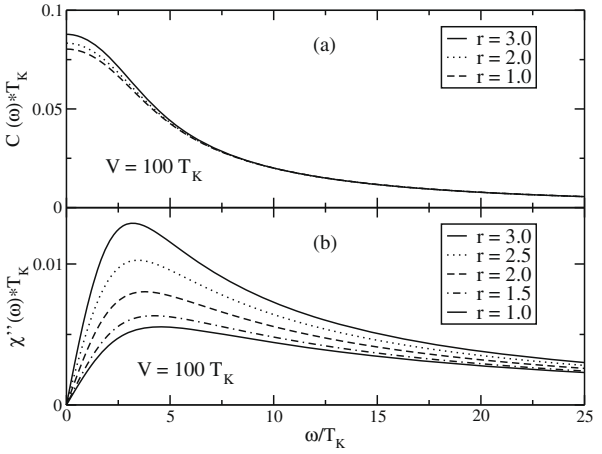

Fig. 13. Universal curves for (a) the spin–spin correlation function $C(\omega)$ and (b) the imaginary part of the dynamical spin susceptibility $\chi''(\omega)$ in non-equilibrium for asymmetric coupling of the leads. The voltage bias is held fixed at $V = 100T_K$.

5.4. Static spin susceptibility

One of the most celebrated results of Kondo physics is the behavior of the static spin susceptibility χ_0 as a function of temperature. This behavior encompasses the screening of the impurity spin via the formation of a Kondo bound state upon lowering temperature. While it is easy to deduce the reduction of the magnetic moment with scaling techniques,

$$\chi_0(T) = \frac{1}{4T}\left(1 - \frac{1}{\ln(T/T_K)}\right), \tag{108}$$

the correct result of a finite non-zero spin susceptibility at zero temperature, $\chi_0(T = 0)$, was first obtained in the seminal application of the numerical renormalization group by Wilson [41]. Later the Bethe ansatz [42,43] gave the complete analytical solution leading to the high temperature expansion

$$\chi_0(T) = \frac{1}{4T}\left(1 - \frac{1}{\ln(T/T_K)} - \frac{\ln(\ln(T/T_K))}{2(\ln(T/T_K))^2} + \mathcal{O}((\ln(T/T_K))^{-2})\right). \tag{109}$$

Likewise, the behavior of the static spin susceptibility as a function of voltage bias is of fundamental importance for understanding non-equilibrium Kondo physics. In the sequel, we will focus on the case of zero temperature, zero magnetic field and non-zero voltage bias. The case of non-zero magnetic field will be discussed in a separate publication. The leading order result for $\chi_0(T,V)$ for large temperature or large voltage bias was worked out by Parcollet and Hooley [44]:

$$\chi_0(T=0,V) = \frac{(1+r)(1+r^{-1})}{4V} = \frac{1}{4T_{\text{eff}}}. \tag{110}$$

This naturally raises the question about the logarithmic corrections to this behavior, similar to the key result (108) of equilibrium Kondo physics. This question has to date only been answered for the leading $\ln^2(V/T_K)$-corrections, which, however, vanish if the Kondo model can be derived from an underlying Anderson impurity model (see Section 2.1). The logarithmic terms proportional to $\ln(V/T_K)$ have not yet been calculated completely, which means that the current status of the non-equilibrium calculation would miss the finite temperature logarithmic correction in equilibrium (108). More details about these calculations and results can be found in [1,2,19] based on perturbative RG and Keldysh techniques.

Within the flow equation framework it is straightforward to derive the leading term (110) *analytically*, but the corrections to it can only be worked out from the full numerical solution of the system of differential equations derived in the previous chapters. Numerical results for the static spin susceptibility obtained in this way via (103) are shown in Figs. 14 and 15.

The comparison (Fig. 14) of the Bethe ansatz result (109) with the flow equation data points in equilibrium as a function of temperature shows very good agreement for large V/T_K. This demonstrates that the flow equation calculation presented here contains the leading logarithmic corrections and can address this issue also in non-equilibrium.

Flow equation results for this non-equilibrium spin susceptibility are plotted in Fig. 14 for symmetric coupling to the leads ($r=1$) as a function of the effective temperature $T_{\text{eff}} = V/4$, Eq. (105). In this way, a direct comparison between equilibrium non-zero temperature and non-equilibrium non-zero voltage bias is possible: naively, one might expect that not only the zeroth-order result (110) can be described by the effective temperature (105), but that this also holds for the logarithmic correction in (108). This is clearly not the case and the logarithmic corrections to $\chi_0(V)$ contain some genuine non-equilibrium physics [45]. Due to numerical limitations, it has unfortunately not been possible to go to larger values of the voltage bias to study the full crossover to the analytically known asymptotic behavior $\lim_{V\to\infty} V\chi_0(V)/4 = 1/4$.

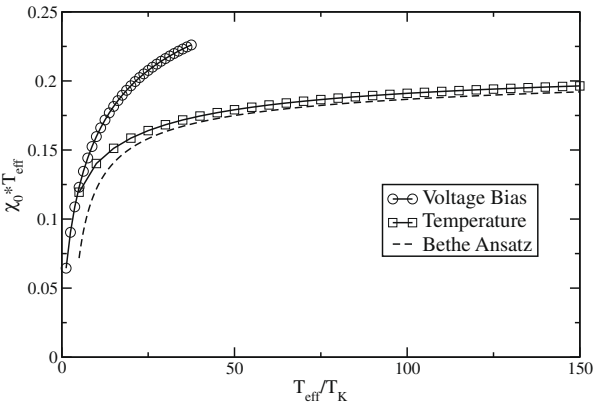

Fig. 14. Flow equation results for the static spin susceptibility χ_0 for non-zero temperature (equilibrium) and for non-zero voltage bias (non-equilibrium, symmetric coupling $r=1$). The data are plotted as a function of the effective temperature $T_{\text{eff}} = V/4$ in the case of voltage bias (while $T_{\text{eff}} \stackrel{\text{def}}{=} T$ for non-zero temperature). For comparison we show the leading order Bethe ansatz result (109) for the equilibrium susceptibility, which agrees very well with the finite temperature flow equation data.

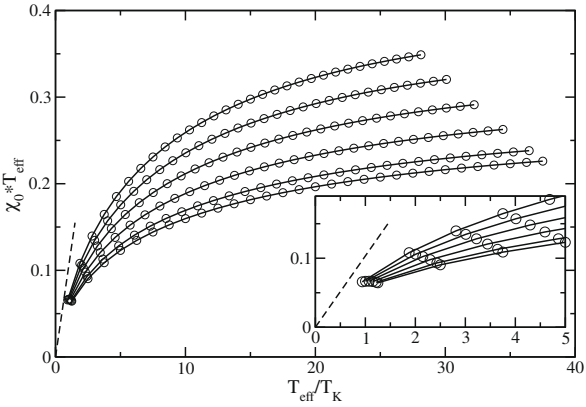

Fig. 15. Flow equation results for the static spin susceptibility χ_0 for non-zero voltage bias for various asymmetry parameters r. The asymmetry parameter increases from bottom to top: $r = 1.0, 1.4, 1.8, 2.2, 2.6, 3.0$. The data are plotted as a function of $T_{\text{eff}} = V/(1+r)(1+r^{-1})$, Eq. (105). The dashed line is an exact result for the behavior in the $T_{\text{eff}} \to 0$ limit independent of r, see text. Lines are guide to the eye only and the numerical error of the data points is at most 10%. The inset shows a blowup of the small voltage bias region.

Fig. 15 contains the non-equilibrium static spin susceptibility plotted in the same way for various values of the asymmetry parameter r. One can see that the logarithmic corrections get even larger for increasing asymmetry. The values of $T_{\text{eff}}\chi_0(T_{\text{eff}})$ clearly start to overshoot the asymptotic value 1/4 for larger asymmetries. As opposed to the equilibrium case, the effective magnetic moment in non-equilibrium first increases upon lowering the voltage bias. This is related to the strong energy-dependence of the running coupling constant in non-equilibrium, see also Figs. 6 and 7. The behavior here is consistent with what one would conjecture based on the analytically known $\ln^2$-corrections for a Kondo model that cannot be derived from an underlying Anderson impurity model. In that case, the energy-dependence of the couplings becomes even larger than here, eventually reaching two-channel Kondo physics behavior. Likewise, the leading logarithmic corrections to the static spin susceptibility are positive [1,2,19], which is reminiscent of our results depicted in Fig. 15.

The behavior of the curves for smaller values of the voltage bias in Fig. 15 has to be interpreted with care, since the running coupling constants become larger and therefore the flow equation calculation less reliable. Still, the fact that the curves for different asymmetries converge for smaller voltage bias has a simple physical interpretation: we know that $\chi_0(V = 0, T = 0) = w/4T_K$ with the Wilson number $w = 0.413$ known exactly from the Bethe ansatz. This result is trivially independent of r. This translates into a constant slope $w/4$ in Fig. 15 (dashed line), which all the other curves have to approach in the limit $V \ll T_K$ independent of r. Notice that our results for the non-equilibrium static spin susceptibility show clear indications of this behavior.

6. Conclusions

This paper has served a twofold purpose. First, we have worked out how the flow equation method can be applied to steady state non-equilibrium impurity models. This was illustrated in detail for the Kondo model with voltage bias. Thereby we have shown how Hamiltonian scaling ideas can be used in non-equilibrium, and how they help to understand the physics qualitatively and also quantitatively. A point of particular importance is the transmutation of marginal terms in the Hamiltonian into irrelevant terms on the energy scale set by the spin relaxation rate, which is generated by the steady state current. This is precisely the effect of decoherence within our Hamiltonian scaling framework.

In addition to these methodological considerations, we have also derived a number of new results for the non-equilibrium spin dynamics in the Kondo model with voltage bias. In this paper, we have focused on the spin dynamics since it contains frequency resolved information about the non-equilib-

rium steady state (as opposed to the steady-state current (9)). For the equilibrium model, the spin dynamics is the key to understanding Kondo physics, and therefore the spin dynamics is a very suitable tool to illustrate the differences between equilibrium and non-equilibrium. In particular, we have calculated the static spin susceptibility in non-equilibrium including its logarithmic corrections for a wide range of voltage bias. Although we had to resort to a numerical solution of the flow equations for this purpose, this is an important step since to date an analytical calculation of this leading correction has not been possible (at least for the experimentally most relevant case of a Kondo model that is derived from an underlying Anderson impurity model).

Scaling ideas are one of the key concepts for understanding equilibrium many-body systems. Likewise, we believe that Hamiltonian scaling ideas like the one presented here can play an equally important role for steady state non-equilibrium problems.

Acknowledgements

We acknowledge valuable discussions with N. Andrei, J. von Delft, A. Mitra, J. Paaske and A. Rosch. This work was supported through SFB/TR 12 of the Deutsche Forschungsgemeinschaft (DFG), the Center for Nanoscience (CeNS) Munich, and the German Excellence Initiative via the Nanosystems Initiative Munich (NIM).

Appendix A. Commutators and normal-ordering

In this appendix, we work out in detail some key commutators that are used throughout our calculations.

A.1. Commutator $[\vec{S}\cdot\vec{s}_{t't},\vec{S}\cdot\vec{s}_{u'u}]$

We use the following fundamental property of the spin-1/2 algebra

$$S^iS^j=\frac{1}{4}\delta_{ij}+\frac{i}{2}\sum_k\epsilon_{ijk}S^k \tag{111}$$

and insert it into the commutator:

$$\begin{aligned}[\vec{S}\cdot\vec{s}_{t't},\vec{S}\cdot\vec{s}_{u'u}]&=\frac{1}{4}\sum_{i,j}(S^iS^jc^\dagger_{t'\alpha}\sigma^i_{\alpha\beta}c_{t\beta}c^\dagger_{u'\mu}\sigma^j_{\mu\nu}c_{u\nu}-S^jS^ic^\dagger_{u'\mu}\sigma^j_{\mu\nu}c_{u\nu}c^\dagger_{t'\alpha}\sigma^i_{\alpha\beta}c_{t\beta})\\&=\frac{i}{8}\sum\epsilon_{ijk}\sigma^i_{\alpha\beta}\sigma^j_{\mu\nu}S^k\left(c^\dagger_{t'\alpha}c_{t\beta}c^\dagger_{u'\mu}c_{u\nu}+c^\dagger_{u'\mu}c_{u\nu}c^\dagger_{t'\alpha}c_{t\beta}\right)+\frac{1}{16}\sum_i(\sigma^i_{\alpha\beta}\sigma^i_{\mu\nu})[c^\dagger_{t'\alpha}c_{t\beta},c^\dagger_{u'\mu}c_{u\nu}]\\&=\frac{i}{8}\sum\epsilon_{ijk}\sigma^i_{\alpha\beta}\sigma^j_{\mu\nu}S^k\left(c^\dagger_{t'\alpha}c_{t\beta}c^\dagger_{u'\mu}c_{u\nu}+c^\dagger_{u'\mu}c_{u\nu}c^\dagger_{t'\alpha}c_{t\beta}\right)+\frac{3}{16}\sum_\alpha\left(\delta_{tu'}c^\dagger_{t'\alpha}c_{u\alpha}-\delta_{t'u}c^\dagger_{u'\alpha}c_{t\alpha}\right).\end{aligned} \tag{112}$$

Next we need to normal-order the fermion terms. We introduce the following expectation values with respect to the non-interacting ground state

$$\begin{aligned}n^+(u)&\stackrel{\text{def}}{=}\langle c^\dagger_{u\alpha}c_{u\alpha}\rangle=n(u),\\n^-(u)&\stackrel{\text{def}}{=}\langle c_{u\alpha}c^\dagger_{u\alpha}\rangle,\end{aligned} \tag{113}$$

which are related by $n^+(u)=1-n^-(u)$ because of $\{c^\dagger_u,c_{u'}\}=\delta_{uu'}$. No summation over α is implied in (113), and the expectation values are obviously independent of α due to spin symmetry (no magnetic field). Then

$$:c^\dagger_{u'\alpha}c_{u\beta}:\stackrel{\text{def}}{=}c^\dagger_{u'\alpha}c_{u\beta}-\delta_{u'u}\delta_{\alpha\beta}n^+(u)\qquad :c_{u\beta}c^\dagger_{u'\alpha}:\stackrel{\text{def}}{=}c_{u\beta}c^\dagger_{u'\alpha}-\delta_{u'u}\delta_{\alpha\beta}n^-(u) \tag{114}$$

and $:c^\dagger_{u'\alpha}c_{u\beta}:=-:c_{u\beta}c^\dagger_{u'\alpha}:$. For normal-ordering of higher-order fermion terms we follow the prescription of Wegner [22] that not only subtracts the ground state expectation values, but also expectation values with respect to lower-order excited states:

$$\begin{aligned}:c^\dagger_{t'\alpha}c_{t\beta}c^\dagger_{u'\mu}c_{uv}:&\stackrel{\text{def}}{=}:c^\dagger_{t'\alpha}c_{t\beta}::c^\dagger_{u'\mu}c_{uv}:-:c^\dagger_{t'\alpha}c_{uv}:\delta_{tu'}\delta_{\beta\mu}n^-(t)+:c^\dagger_{u'\mu}c_{t\beta}\\&:\delta_{t'u}\delta_{\alpha v}n^+(u)-\delta_{t'u}\delta_{tu'}\delta_{\alpha v}\delta_{\beta\mu}n^-(t)n^+(u).\end{aligned}\tag{115}$$

Inserting everything into (112) yields after some straightforward algebra

$$\begin{aligned}[\vec S\cdot\vec s_{t't},\vec S\cdot\vec s_{u'u}]=i:\vec S\cdot(\vec s_{t't}\times\vec s_{u'u}):&+\vec S\cdot\vec s_{t'u}\delta_{tu'}(n^+(t)-1/2)-\vec S\cdot\vec s_{u't}\delta_{t'u}(n^+(u)-1/2)\\&+\frac{3}{16}\sum_\alpha\left(\delta_{tu'}:c^\dagger_{t'\alpha}c_{u\alpha}:-\delta_{t'u}:c^\dagger_{u'\alpha}c_{t\alpha}:\right)+\frac{3}{8}\delta_{tu'}\delta_{t'u}(n^+(u)-n^+(t)).\end{aligned}\tag{116}$$

Normal-ordering in the first term on the rhs of this equation acts on the fermions only

$$:\vec S\cdot(\vec s_{t't}\times\vec s_{u'u}):=\vec S\cdot:(\vec s_{t't}\times\vec s_{u'u}):.\tag{117}$$

A.2. Commutator $[:\vec S\cdot(\vec s_{1'1}\times\vec s_{2'2}):,\vec S\cdot\vec s_{4'4}]$

For notational clarity, we use labels $1',1,2',2,4',4$ instead of v',v,w',w,u',u in this section. For the purposes of this paper, we also only need to identify terms with the structure $\vec S\cdot\vec s_{t't}$ in the above normal-ordered commutator. This will simplify our calculation considerably.

Using (111), it is easy to show

$$[:\vec S\cdot(\vec s_{1'1}\times\vec s_{2'2}):,\vec S\cdot\vec s_{4'4}]=\frac14\sum_{a=1}^3[:(\vec s_{1'1}\times\vec s_{2'2})^a:,s^a_{4'4}]+\frac{i}{2}\sum_{a,b,c=1}^3\epsilon_{abc}S^c\{:(\vec s_{1'1}\times\vec s_{2'2})^a:,s^b_{4'4}\}.\tag{118}$$

The first term does not contain the impurity spin and can therefore not contribute to the terms that we need to extract from the commutator. We can focus on the anticommutator in the second term

$$\sum\nolimits_{a,b=1}^3\epsilon_{abc}\{:(\vec s_{1'1}\times\vec s_{2'2})^a:,s^b_{4'4}\}=\sum_{i=1}^3\{:s^i_{1'1}s^c_{2'2}:,s^i_{4'4}\}-\sum_{i=1}^3\{:s^c_{1'1}s^i_{2'2}:,s^i_{4'4}\}.\tag{119}$$

In order to yield terms with the structure $\vec S\cdot\vec s_{t't}$, we need to extract the terms with two contractions (i.e., two $n^\pm$-terms) in (119). Similar to (115), one shows

$$\begin{aligned}:c^\dagger_{1'}c_1c^\dagger_{2'}c_2::&=:(0-\text{contraction}):+:(1-\text{contraction}):+\delta_{1'4}\delta_{14'}n^+(1')n^-(1)\\&:c^\dagger_{2'}c_2:+\delta_{2'4}\delta_{24'}n^+(2')n^-(2):c^\dagger_{1'}c_1:-\delta_{1'4}\delta_{24'}n^+(1')n^-(2):c^\dagger_{2'}c_1\\&:-\delta_{2'4}\delta_{14'}n^+(2')n^-(1):c^\dagger_{1'}c_2:.\end{aligned}\tag{120}$$

From this expression, it is straightforward to show

$$\begin{aligned}\sum_{i=1}^3:s^i_{1'1}s^c_{2'2}:s^i_{4'4}=&:(0-\text{contraction}):+:(1-\text{contraction})\\&:+\delta_{1'4}\delta_{14'}n^+(1')n^-(1)\frac32s^c_{2'2}+\delta_{2'4}\delta_{24'}n^+(2')n^-(2)\frac12s^c_{1'1}-\delta_{1'4}\delta_{24'}n^+(1')n^-(2)\frac34s^c_{2'1}\\&-\delta_{2'4}\delta_{14'}n^+(2')n^-(1)\frac34s^c_{1'2}.\end{aligned}$$

Combining all the like terms in (119) yields

$$\begin{aligned}\sum_{a,b=1}^3\epsilon_{abc}\{:(\vec s_{1'1}\times\vec s_{2'2})^a:,s^b_{4'4}\}=&:(0-\text{contraction}):+:(1-\text{contraction})\\&:+\delta_{1'4}\delta_{14'}(n^+(1')n^-(1)+n^+(1)n^-(1'))s^c_{2'2}-\delta_{2'4}\delta_{24'}(n^+(2')n^-(2)+n^+(2)n^-(2'))s^c_{1'1}.\end{aligned}\tag{121}$$

This gives our desired result by inserting into (118)

$$\begin{aligned}&[:\vec{S}\cdot(\vec{s}_{1'1}\times\vec{s}_{2'2}):,\vec{S}\cdot\vec{s}_{4'4}]\\&=\frac{i}{2}\delta_{1'4}\delta_{14'}(n^+(1')n^-(1)+n^+(1)n^-(1'))\vec{S}\cdot\vec{s}_{2'2}-\frac{i}{2}\delta_{2'4}\delta_{24'}(n^+(2')n^-(2)+n^+(2)n^-(2'))\vec{S}\\&\quad\cdot\vec{s}_{1'1}+\text{normal}-\text{ordered terms with different structure.}\end{aligned}\tag{122}$$

A.3. Numerical solution

This appendix contains some details of the numerical solution of the full set of flow equations (52) and (53). The latter are solved using a standard Runge–Kutta algorithm [46].

One numerical issue arises from the fact that the K-couplings in (48) depend on four momenta which leads to a large number of differential equations to keep track of. While this is no fundamental problem, it would limit the possible resolution on a standard workstation considerably. However, one can use the following approximation which reduces the complexity to quadratic in the number of momenta and provides an excellent approximation to the full system.

The formal solution of (53) is given by

$$K_{p'p,q'q}=-(\epsilon_{q'}-\epsilon_q)e^{-B(\epsilon_{p'}-\epsilon_p+\epsilon_{q'}-\epsilon_q)^2}\int_0^B d\widetilde{B}e^{\widetilde{B}(\epsilon_{p'}-\epsilon_p+\epsilon_{q'}-\epsilon_q)^2}J_{p'p}(\widetilde{B})J_{q'q}(\widetilde{B}).\tag{123}$$

Using this result, the flow equations for the running coupling (52) in diagonal parametrization

$$J_{p'p}=u_{\overline{p'p}}e^{-B(\epsilon_{p'}-\epsilon_p)^2}\tag{124}$$

are easily rewritten to the form

$$\begin{aligned}\frac{du_p}{dB}=&\sum_q(\epsilon_p-\epsilon_q)u^2_{\overline{pq}}e^{-2B(\epsilon_p-\epsilon_q)^2}(2n_f(q)-1)-\sum_{q',q}(n_f(q')+n_f(q)-2n_f(q')n_f(q))\\&\times(\epsilon_{q'}-\epsilon_q)^2e^{-2B(\epsilon_{q'}-\epsilon_q)^2}u_{\overline{q'q}}L_{p,\overline{q'q}},\end{aligned}\tag{125}$$

where

$$L_{p',p}=\int_0^B d\widetilde{B}\,u_{p'}(\widetilde{B})u_p(\widetilde{B}).\tag{126}$$

In the remaining flow equations, for example the transformation of the spin operator, the running coupling $J_{p'p}(B)$ is simply replaced by the rhs of (124). The equations above can be easily generalized to the case of general parameters (47) and (48).

Using diagonal parametrization in the numerical solution effectively reduces the number of differential equations to quadratic in the number of momenta N. The runtime is proportional to N^3 instead of N^4 in the full set. Additionally, the stiffness of the differential equations is reduced by removing the exponential decay from the flow of the running coupling. On a standard workstation N can be chosen of $\mathcal{O}(1000)$.

References

[1] A. Rosch, J. Paaske, P. Wölfle, Phys. Rev. Lett. 90 (2003) 076804.
[2] A. Rosch, J. Paaske, J. Kroha, P. Wölfle, J. Phys. Soc. Jpn. 74 (2005) 118.
[3] H. Schoeller, Lect. Notes Phys. 544 (2000) 137.
[4] S.G. Jakobs, V. Meden, H. Schoeller, Phys. Rev. Lett. 99 (2007) 150603.
[5] A. Mitra, A.J. Millis, Phys. Rev. B 76 (2007) 085342.
[6] D. Segal, D.R. Reichman, A.J. Millis, Phys. Rev. B 76 (2007) 195316.
[7] S. Kehrein, Phys. Rev. Lett. 95 (2005) 056602.
[8] A. Hackl, S. Kehrein, Phys. Rev. B 78 (2008) 092303. arXiv:0809.3524.
[9] D. Goldhaber-Gordon et al, Nature 391 (1998) 156.
[10] S.M. Cronenwett, T.H. Oosterkamp, L.P. Kouwenhoven, Science 281 (1998) 540.
[11] J. Schmid, J. Weis, K. Eberl, K. von Klitzing, Physica B 258 (1998) 182.

[12] W.G. van der Wiel et al, Science 289 (2000) 2105.
[13] L. Glazman, M. Raikh, JETP Lett. 47 (1988) 452.
[14] T. Ng, P.A. Lett, Phys. Rev. Lett. 61 (1988) 1768.
[15] F.B. Anders, Phys. Rev. Lett. 101 (2008) 066804.
[16] E. Boulat, H. Saleur, P. Schmitteckert, Phys. Rev. Lett. 101 (2008) 140601.
[17] P. Mehta, N. Andrei, Phys. Rev. Lett. 96 (2006) 216802;
P. Mehta, Sung po Chao, N. Andrei, arXiv:cond-mat/0703426.
[18] A. Kaminski, Yu.V. Nazarov, L.I. Glazman, Phys. Rev. Lett. 83 (1999) 384;
Phys. Rev. B 62 (2000) 8154.
[19] J. Paaske, A. Rosch, P. Wölfle, Phys. Rev. B 69 (2004) 155330.
[20] J. Paaske, A. Rosch, J. Kroha, P. Wölfle, Phys. Rev. B 70 (2004) 155301.
[21] A. Rosch, J. Kroha, P. Wölfle, Phys. Rev. Lett. 87 (2001) 156802.
[22] F. Wegner, Ann. Physik (Leipzig) 506 (1994) 77.
[23] S. Głazek, K.G. Wilson, Phys. Rev. D 48 (1993) 5863;
S. Głazek, K.G. Wilson, Phys. Rev. D 49 (1994) 4214.
[24] S. Kehrein, The Flow Equation Approach to Many-Particle Systems, Springer, Berlin, 2006.
[25] S. Kehrein, Phys. Rev. Lett. 83 (1999) 4914;
Nucl. Phys. B[FS] 592 (2001) 512.
[26] W. Hofstetter, S. Kehrein, Phys. Rev. B 63 (2001) 140402(R).
[27] P.W. Anderson, J. Phys. C 3 (1970) 2436.
[28] P. Coleman, C. Hooley, P. Parcollet, Phys. Rev. Lett. 86 (2001) 4088.
[29] S. Kehrein, A. Mielke, Ann. Physik (Leipzig) 6 (1997) 90.
[30] S. Kleff, S. Kehrein, J. von Delft, Phys. Rev. B 70 (2004) 014516.
[31] I. Grote, E. Körding, F. Wegner, J. Low Temp. Phys. 126 (2002) 1385;
V. Hankevych, I. Grote, F. Wegner, Phys. Rev. B 66 (2002) 094516.
[32] C. Knetter, K.P. Schmidt, M. Grüninger, G.S. Uhrig, Phys. Rev. Lett. 87 (2001) 167204;
C. Knetter, K.P. Schmidt, G.S. Uhrig, Eur. Phys. J. B 36 (2004) 525.
[33] M. Garst et al, Phys. Rev. B 69 (2004) 214413.
[34] M. Moeckel, S. Kehrein, Phys. Rev. Lett. 100 (2008) 175702.
[35] D. Lobaskin, S. Kehrein, Phys. Rev. B 71 (2005) 193303.
[36] Notice that it is possible to have flow equation expansion parameters different (i.e., more well-behaved) from the running coupling constants, which is the reason why flow equations can yield a controlled expansion even in certain strong-coupling problems [25,26].
[37] For an overview see, e.g. A.C. Hewson, The Kondo Problem to Heavy Fermions, Cambridge University Press, Cambridge, 1993.
[38] One can work this out easily from (31) and (32) with finite temperature Fermi functions $n(u)$.
[39] The differential equations for u_t, u_l, u_r correspond to Eqs. (5) and (6) in Ref. [7].
[40] H.B. Callen, T.A. Welton, Phys. Rev. 83 (1951) 34.
[41] K.G. Wilson, Rev. Mod. Phys. 47 (1975) 773.
[42] V.M. Filyov, A.M. Tzvelik, P.B. Wiegmann, Phys. Lett. A 81 (1981) 175.
[43] N. Andrei, J.H. Lowenstein, Phys. Rev. Lett. 46 (1981) 356.
[44] O. Parcollet, C. Hooley, Phys. Rev. B 66 (2002) 085315.
[45] Another way of saying this is to argue that the effective temperature acquires logarithmic corrections in non-equilibrium. However, one would need to check other observables to verify whether this notion is useful.
[46] See e.g. W.H. Press et al, Numerical Recipes, third ed., Cambridge University Press, Cambridge, 2007.